# Land-use evolution in the catchment of Lake Murten, Switzerland

Mischa Haas[1,2] Petra Kaltenrieder[3,4], S. Nemiah Ladd[1,2], Caroline Welte[5], Michael Strasser[6], Timothy Ian Eglinton[2], Nathalie Dubois[1,2]

[1]Swiss Federal Institute of Aquatic Science and Technology (Eawag), CH-8600 Dübendorf

[2]Department of Earth Sciences, ETH Zürich, CH-8006 Zürich

[3]Institute of Plant Sciences, University of Bern, CH-3012 Bern

[4]Oeschger Center for Climate Change Research, University of Bern, CH-3012 Bern

[5]Laboratory of Ion Beam Physics, ETH Zürich, CH-8006 Zürich

[6]Department of Geology, Universität Innsbruck, AT-6020 Innsbruck

***Corresponding Author:*** mischa.haas@eawag.ch

***Highlights:***

- Pollen and leaf waxes from Lake Murten record land-use evolution since prehistory
- Large-scale Roman deforestation and farming around the city of Aventicum
- Land-use and vegetation recovery times following Roman disturbance took centuries

***Abstract:***

Anthropogenic soil erosion is a problem of global concern and recently has become the focus of extensive research. In spite of this, our knowledge about the history of land-use and its long-term impact on soil erosion and the local environment remains limited. This study seeks to address this issue by investigating sediments of Lake Murten, Switzerland, using a multi-proxy approach to reconstruct the history of land-use and its impacts in the catchment. We analyzed pollen and charcoal to reconstruct past land-use and vegetation dynamics, and used the distributions of terrestrial leaf wax biomarkers, their $\delta^{13}C$ isotopic composition and their soil retention time (compound-specific $^{14}C$) to evaluate long-term effects on past soil carbon dynamics.

Arboreal pollen abundances, charcoal influx and cultural indicators match the archaeological evidence and reveal an eventful past around the lake. The first signs of human presence were detected around 5000 BCE, when Neolithic pile dwellers occupied the lake's shores. However, human land-use had no significant effect on the pollen and the sedimentary organic matter (OM) composition during Neolithic times and the Bronze Age. This changed during the Late Iron Age and the Early Roman Period (ca. 70 BCE). Coincident with the rise of *Aventicum,* a Roman city, large-scale deforestation and agriculture began in the region. Severe soil degradation and outwash of soil organic carbon (SOC) at this time is documented by enhanced input of soil-derived and pre-aged leaf waxes, and resulted in cultural eutrophication ca. 2000 years ago. Soil erosion decreased after the fall of the Roman Empire and a short period of renaturation followed. Although the export of SOC returned to pre-Roman values after ca. 200 years, the forest never recovered to its past extent. The last two detected periods of land-use change correlate with the onset of Medieval agriculture (ca. 1000 CE) and the Industrial Period (ca. 1800 CE). Today, the mean transit time of leaf waxes is almost five times longer compared to the Roman Period, suggesting that substantial soil erosion has occurred and that an even longer time period would be necessary for the soil carbon dynamics to recover to their natural state.

---

***Key words:*** Land-use Reconstruction, Pollen, Charcoal, Leaf Waxes, Compound-Specific $\delta^{13}C$, Compound-Specific Radiocarbon Dating

## *1. Introduction*

Soil erosion as a consequence of human land-use is a pervasive problem of global concern (Lal, 2004; Quinton et al., 2010). Land-clearing, field cultivation and pastoralism are considered to be the land-use activities that are the most influential drivers of soil erosion. Such landscape modifying activities do not only have direct physical impacts on soils, but also have indirect impacts, including changes in local carbon dynamics (Foster et al., 2003). Soil organic carbon (SOC) is the largest terrestrial carbon reservoir on Earth (Quinton et al., 2010) and the magnitude of the changes in local carbon dynamics due to the mobilization, transport and redistribution of SOC has been much-debated in the context of land-use change (Lal, 2005; Van Oost et al., 2007). In particular, our knowledge of the long-term impact of soil degradation and its historical

55 evolution is rather limited. Past land-use and its legacy can influence terrestrial and aquatic ecosystems,
56 including ecological functions, for centuries or even longer (Foster et al., 2003). Analyzing soil erosion rates
57 in a historical to pre-historical context allows pre-anthropogenic conditions, the long-term influence of
58 intensive land-use periods and the effects of renaturation periods to be evaluated.
59
60 Sedimentary repositories are promising archives that can be used to improve our understanding of the
61 relationship between land-use history and SOC dynamics. Terrestrial archives integrating a catchment wide
62 signal, such as lake or peat sediments, are natural recorders of environmental change and can be used to study
63 soil erosion in a historical perspective (Huang and O'Connell, 2000). During phases of human land-use, i.e.
64 activities that modify landscapes, the structure of top- and subsoil gets destroyed (Lal, 2002). As a
65 consequence minerogenic and chemical erosional products from the impacted catchment soils, including SOC,
66 are mobilized and often compiled in sedimentary repositories such as lakes (Edwards and Whittington, 2001).
67 Previous studies have documented that organic matter (OM) and specific organic fractions deposited during
68 land-use periods differ significantly in their bulk geochemical properties and in their isotopic composition
69 compared to the material deposited as background sedimentation during undisturbed periods (Enters et al.,
70 2006; Meyers, 1994). However, sedimentary OC is very heterogeneous and contains carbon from diverse
71 allochthonous and autochthonous sources of both geological and biological origin (Gierga et al., 2016), which
72 dilutes the initial SOC signal and can make it difficult to identify periods of land-use change from the
73 properties of bulk soil alone.
74
75 In the last decades, new attempts to address the complications regarding the heterogeneity of sedimentary OC
76 have been developed with a focus on source-specific organic compound classes of terrestrial origin (Douglas
77 et al., 2018; Galy et al., 2011). In general, only a low percentage of eroded terrestrial OC is permanently
78 buried in the sedimentary record due to early diagenesis and microbial consumption during transit and initial
79 deposition (Vonk et al., 2010). This leads to the selective preservation of organic compounds with relatively
80 recalcitrant molecular structures and affiliation to mineral matrices (Vonk et al., 2010). Among the
81 compounds that are particularly well preserved in sediments, leaf wax lipids that are predominantly produced
82 by higher terrestrial plants are among the most studied. These long-chain *n*-alkanes and *n*-carboxylic acids

have a persistent molecular structure and are well-represented in the refractory SOC pool (Douglas et al., 2018; Feng et al., 2013; Smittenberg et al., 2006).

By analyzing leaf wax molecular distributions, isotopic compositions and relative ages, it is possible to gain specific information not only about the paleoenvironment that prevailed during the time of synthesis but also about their past (and current) retention times in soils (Douglas et al., 2018; Dubois and Jacob, 2016). In recent studies, compound-specific radiocarbon analyses (CSRA) of leaf waxes from lake sediments has confirmed that periods of land-use have long-lasting effects on soil carbon dynamics (Douglas et al., 2018, 2014; Gierga et al., 2016). In these studies, the relative retention or transit time of leaf waxes provided an estimate of soil stability through time. However, in order to clearly identify anthropogenic effects and to exclude natural background erosion, additional independent proxies, such as the study of pollen and non-pollen palynomorphs, can provide important environmental context.

Pollen, spores and non-pollen palynomorphs retrieved from lake sediment are frequently used to estimate relative changes in vegetation cover within the catchment or to identify land-use periods. Palynological proxies have emerged as a robust tool to trace paleoecological changes (Bichet et al., 2013; Hillbrand et al., 2014; Tinner et al., 2003). Periods of human land-use are often associated with significant increases in the charcoal influx due to fire activity and with the occurrence of a variety of cultural indicator species, such as Cerealia type and *Plantago lanceolata* pollen or spores of coprophilous fungi (Behre, 1988; Cugny et al., 2010; Tinner et al., 2003; van Geel et al., 2003).

In a previous publication we detected drastic increases in soil erosion indicators correlating with the timing of Roman land-use 2000 years ago and the Industrial Period (Haas et al., 2019). Building on this framework, we applied in the current study a more source-specific approach based on pollen and leaf wax data in order to reconstruct the evolution of land-use and its impact on soil degradation in the catchment of Lake Murten, for the past 8000 years.

First, we analyzed the distribution of pollen in the sedimentary record to develop an overview of the regional to local vegetation history, to identify human activities, and to assess paleoecological changes triggered by

111 human land-use. Second, we estimated the influence of human land-use on local carbon dynamics in a pre-
112 historical to historical context, using the distribution, isotopic composition ($\delta^{13}C$ values) and relative ages
113 (CSRA) of terrestrial leaf waxes. This allowed us to evaluate not only the long-term influence of intensive
114 land-use periods on soil degradation, but also to investigate pre-anthropogenic conditions and effects of
115 renaturation periods on the local carbon dynamics.
116
117 *1.1. Study Site*
118 Lake Murten is situated in the lowlands of western Switzerland, also known as the Swiss Plateau region
119 (Figure 1). The catchment has – geologically spoken - a relatively mixed bedrock composition, with various
120 conglomerates, sandstones, clays and marls (Pfiffner, 2014). The hillsides, such as Mont Vully, are glacially
121 imprinted side moraines. Towards the south of the lake lies the alluvial plain of the La Broye river,
122 representing the main inflow to the lake.
123
124 ***Figure 1:*** Location of Lake Murten (Switzerland). Locations of human settlements around the lake from the
125 Neolithic to the Medieval Period are indicated by the colored regions, and gray shading represents local
126 topography (Castella et al., 2015; Nast, 2006; UNESCO Palafittes, 2015). Data source: swisstopo (Art. 30
127 GeoIV): 5704 000 000 / swissTLM3D@2011, DHM25@2003, Vector200©2011, reproduced with permission
128 of swisstopo / JA100119.
129
130 The Swiss Plateau region is rich in archaeological sites from several periods of human activity. The shores of
131 Lake Murten have a remarkably dense history of settlement and cultural activities (Figure 1). Beginning 7000
132 - 6000 years ago, Neolithic pile dweller communities lived by Lake Murten (Menotti, 2004; UNESCO
133 Palafittes, 2015) and their sedentary lifestyle dominated the shores of the lake for millennia. In the Late Iron
134 Age (La Tène cultural period, 450 – 20 BCE), large-scale deforestation and farming first occurred in the
135 catchment area as the population became more dense and centralized. Architectural remnants of this Celtic era
136 include the remains of a fortress (lat. *oppidum*) on Mont Vully, overlooking the area of Lake Murten and Lake
137 Neuchâtel (Nast, 2006) (Figure 1).
138

139 The Romans made their entrance to the Swiss Plateau in the 1st century before the Common Era (BCE).
140 Numerous ruins and excavations in and around the village of Avenches provide evidence of an influential
141 Roman city called *Aventicum*, capital of the Helvetians, within close proximity to the lake. At the peak of its
142 influence (2nd century common era, CE) *Aventicum* contained approximately 20,000 inhabitants, which led to
143 further large-scale deforestation and agriculture in the region (Castella et al., 2015). After the fall of the
144 Roman Empire (5th century CE), the Great Migration Period led to socio-economic changes that contributed to
145 a decentralization of the population. Archaeological findings from this period are rare in the vicinity of Lake
146 Murten.
147
148 Starting in the Early Medieval Period (ca. 11th century CE) human activity in Switzerland intensified (Egli,
149 1988). The foundation and construction of the first Medieval fortress in Murten by the Burgundians began in
150 the year 814 CE (Schöpfer, 2016). The city of Murten remains the largest conurbation in the catchment today.
151 The Industrial Period was characterized by several water-corrections and drainage of the swamp area north of
152 the lake, paving the way for intensive agriculture (Nast, 2006).
153
154 In a previous study we showed that drastic increases in soil erosion indicators such as relative X-ray
155 fluorescence titanium (XRF Ti) concentrations, magnetic susceptibility (MS) and sediment mass accumulation
156 rates (MAR) were correlated with the timing of Roman land-use 2000 years ago and the Industrial Period
157 (Haas et al., 2019). The bulk sediment $^{14}C$ time series that was previously established (Haas et al., 2019)
158 offers an ideal base for our present study. Increasing age-offsets between bulk sedimentary organic carbon and
159 the modeled deposition age revealed terrestrial runoff of pre-aged SOC due to human induced soil erosion.
160 Interestingly, with the end of the Roman Period and relaxation of human pressure, soil erosion indicators
161 including the bulk sediment age offsets decreased and reached steady conditions around 200 years after
162 human activity ceased, which was interpreted as a period of renaturation and soil stabilization (Haas et al.,
163 2019).
164
165 In the present study we worked on the same sedimentary record. Here, we add a new palynological data set
166 that allows us to expand our knowledge about the vegetation dynamics and history of agriculture in the

167 catchment and to clearly identify land-use activity. Our present paleoecological overview compares well with
168 former palynological work at Lake Murten (Hadorn, 1984). In addition, in the present study we focused on
169 specific leaf waxes of terrestrial origin, which ensures better source control than the bulk SOC studied
170 previously, and allows us to draw direct conclusions about the impact of land-use and abandonment on soil
171 carbon dynamics.
172
173 ***2. Material and Methods***
174 *2.1. Chronology*
175 The chronology of the Lake Murten sediment record (Latitude: 46.929220, Longitude: 7.067460, Haas et al.,
176 2019) is based on 25 radiocarbon dates on terrestrial macrofossils, varve counting and $^{137}$Cs radionuclide
177 dating. Compared to the age-depth model of Haas et al. (2019), 15 additional radiocarbon ages on terrestrial
178 plant macrofossil were obtained (Figure 2, appendix A). We followed the procedure of Haas et al. (2019) to
179 prepare the additional macrofossil assemblages for radiocarbon dating on an EA-AMS (MICADAS, ETH
180 Zürich). Furthermore, the sampling error was estimated using the sample thickness and the average
181 sedimentation rate of approximately 8 years/cm (y/cm) and added to the analytical error of the radiocarbon
182 dates using error propagation (see appendix A). Instead of classic (linear) age-depth modeling as used in Haas
183 et al. (2019) (clam by Blaauw, 2010), we used a new approach using Bayesian statistics to reconstruct
184 sediment accumulation rates for sediment records, implemented in the program BACON (Blaauw and
185 Christen, 2011). BACON subdivides a sediment record into numerous vertical sections and estimates the
186 sedimentation rate (in y/cm) using millions of Markov Chain Monte Carlo (MCMC) iterations. The model
187 was calculated with a mean sedimentation rate (acc.mean) of 5 y/cm and an “accumulation shape” (acc.shape)
188 of 1.5 on 101 sections of 10 cm thickness (Figure 2). Ages in this article are reported as Before Common Era
189 (BCE) and Common Era (CE), respectively.
190
191 The application of this new age model resulted in larger confidence intervals, and some events described in
192 our previous publication (Haas et al., 2019) became older by approximately a 100 years. All interpreted events
193 and changes described in Haas et al. (2019), however, fall into the 95% confidence interval (CI) of the
194 updated age-model and thus retain their significance.

195

196 ***Figure 2:*** A. Age-depth model of the Lake Murten sediment record based on varve counting, radionuclide
197 $^{137}Cs$ and radiocarbon dating on macrofossils. The lithological description follows Haas et al. (2019).
198 Abbreviations: Mesolithic Period (MP), Iron Age (IA), Bronze Age (BA), confidence interval (CI). B.
199 Enlarged zoom of the top 40 cm of the core. C. and D. prior (green) and posterior (grey) distributions of the
200 sedimentation rate and memory, respectively, that were used in the program BACON (appendix A) for age-
201 depth modelling (Blaauw and Christen, 2011).

202

203 *2.2. Pollen, spore and microscopic charcoal analysis*

204 The palynological results are presented in percentages of the terrestrial pollen sum (Fig. 3, appendix B).
205 Laboratory treatment followed standard preparation procedures for glycerin samples after Moore et al. (1991).
206 Lycopodium tablets were added to the samples prior to chemical and physical treatment in order to estimate
207 pollen and charcoal concentrations (grains or particles/$cm^3$) and charcoal influx (particles/$cm^2$/year,
208 Stockmarr, 1971). Pollen, spores and microscopic charcoal particles from 40 samples (1 $cm^3$) were analyzed.
209 In each of these, a pollen sum of >500 terrestrial pollen grains (except sample at 317.5 cm) per sample were
210 counted. The pollen results are presented in percentages calculated on the terrestrial pollen sum. Pollen grains,
211 spores and other non-pollen palynomorphs (NPP) were identified using palynological keys and photo
212 references (Beug, 2004; Moore et al., 1991; Reille, 1995). Coprophilous fungal spores were identified
213 following van Geel et al. (2003). Microscopic charcoal particles were counted according to Finsinger and
214 Tinner (2005) and Tinner and Hu (2003). In total, 146 palynological taxa were identified in the sedimentary
215 record of Lake Murten. The results (counts) were normalized relative to the total pollen sum and displayed as
216 percentages. The pollen record was subdivided into three statistically significant local pollen assemblage
217 zones (PMUR-1-3) using constrained clustering, implemented in the program ZONE 1.2 (Juggins, 1991), and
218 the broken stick model (BSTICK) to determine the number of statistically significant zones (Bennett, 1996). A
219 diagram with a selection of the most important pollen, spore and non-pollen palynomorphs for the
220 paleoecological overview and the discussion of land-use activity can be found in the appendix B.

221

222 *2.3. Leaf Wax Extraction, Purification and Quantification*

223 Total lipid extracts (TLEs) were obtained from ~10g of freeze-dried, ground, and homogenized sediment from
224 each selected depth using a microwave extraction system (Milestone, MLS 1200 mega) with 10 - 15 ml of
225 10% methanol in dichloromethane (DCM) (2 min with 300 W from room temperature to 70°C and 5 min with
226 500 W at 70°C). The TLE was eluted over an aminopropyl column (1 g, Sigma Aldrich, LC-NH2 SPE Bulk)
227 with different solvents of increasing polarity. The first fraction (containing *n*-alkanes) was eluted with 10 ml
228 of *n*-hexane, the second fraction with 4 ml of 20% DCM in *n*-hexane, the third fraction with 4 ml of 10%
229 acetone in DCM and the fourth fraction (containing *n*-carboxylic acids) with 2% formic acid in DCM.
230
231 The fractions containing *n*-carboxylic acids were derivatized to form fatty acid methyl esters (FAMEs) using
232 10 ml of 5% hydrochloric acid (32%) in methanol and heated at 70°C for 12 h. The organic phase was
233 recovered by liquid-liquid extraction with *n*-hexane. The resulting FAMEs were purified with a silver nitrate
234 coated silica gel pipette column (0.4 g, Sigma Aldrich) using different solvents of increasing polarity. The first
235 fraction was eluted with 2 ml of *n*-hexane and the second fraction (containing the saturated *n*-carboxylic acid
236 FAMEs), with 4.5 ml of 20% DCM in *n*-hexane.
237
238 The fractions containing *n*-alkanes were purified using a zeolite pipette column (0.2 g, Geokleen,
239 GHGeochemical Services) with *n*-hexane following the method of Haas et al. (2017). Aliquots of the purified
240 *n*-alkane and *n*-carboxylic acid samples were analyzed by gas chromatography mass spectrometry (GC-MS,
241 5977B MSD, Agilent Technologies) and quantified for their concentrations, average chain lengths (ACL, after
242 Poynter and Eglinton (1990)) and carbon preference indices (CPI, after Bray and Evans (1961)) on the GC-
243 MS using the flame ionization detector (FID) attached to the same instrument. To minimize $^{14}C$ contamination
244 only external *n*-alkane ($nC_{7\text{-}40}$) and *n*-carboxylic acid standards ($nC_{16+22+24+28}$) were used for quantification. A
245 summary of the leaf wax data is added in the appendix C.
246
247 *2.4. Compound-specific radiocarbon dating*
248 Nine samples with highest concentrations of leaf waxes were selected for compound specific radiocarbon
249 dating. Specific *n*-alkane homologues *n*-$C_{27}$, *n*-$C_{29}$, *n*-$C_{31}$, *n*-$C_{33}$ and *n*-$C_{35}$ were collected using a GC-FID
250 (7890B, Agilent Technologies) coupled to a preparative fraction collector (PFC, Gerstel). The individual

compound fractions were recovered from the PFC glass traps by elution with 1 ml *n*-hexane. Column bleed was removed by eluting the samples with *n*-hexane over a silica gel pipette column (0.1 g, Fluka Analytical). The transfer of the compound fraction into an EA tin capsule (Säntis AG) was performed by repetitive dissolution and transfer with DCM. A heat plate (37°C) was used to evaporate the DCM. To obtain sufficient quantities for radiocarbon dating, several compound fractions needed to be pooled (13 samples for CSRA) and in some cases the bulk *n*-alkane fraction, containing every chain length, was used for radiocarbon dating (19 bulk *n*-alkane samples). A sample list including the radiocarbon results is given in appendix D.

Radiocarbon analyses of the *n*-alkane fractions were performed on an accelerated mass spectrometer (AMS) equipped with an elemental analyser (EA) at the Laboratory for Ion Beam Physics of ETH Zürich, Switzerland (MICADAS, Wacker et al., 2013). To monitor recoveries and $^{14}C$-backgrounds, specific *n*-alkane standards (*n*-$C_{28}$ and *n*-$C_{32}$) with known $^{14}C$-concentration (Fm of 0 and Fm of 1.073, respectively) were processed. Samples that went through compound separation (GC-PFC) were corrected for the constant background contamination with GC-PFC processed *n*-$C_{28}$ and *n*-$C_{32}$. Bulk *n*-alkane fractions were corrected with unprocessed *n*-$C_{28}$ and *n*-$C_{32}$. A constant contamination correction was applied according to Hanke et al. (2017)(A summary of the compound-specific radiocarbon data is given in appendix E). Based on the blank assessment only data with errors (Fm) < 8% and sample masses larger than 10 µg of carbon were taken into account for the discussion.

All radiocarbon ages were calibrated with IntCal 13 (Reimer et al., 2013). Specific ages in this article are calibrated and represent the 95% confidence interval and median age. The results were compared with the macrofossil based age model and bulk sediment ages from Haas et al. (2019) and 15 additional measurements following the same procedure (Figure 2, appendix F). The mean transit time (MTT) represents the difference between the bulk sediment age (Median) and the *n*-alkane age (Median) to the age model (i.e. sedimentation age) and is reported in years. MTT errors were calculated using error propagation (appendix E).

### *2.5. Compound-specific $\delta^{13}C$ isotope analysis*

278 FAME and *n*-alkane $\delta^{13}C$ values were determined by gas chromatography – isotope ratio mass spectrometry
279 (GC-IRMS) at Eawag's Center for Ecology, Evolution and Biogeochemistry in Kastanienbaum, Switzerland.
280 A GC-1310 (Thermo Scientific, Bremen, Germany) was interfaced to a Delta Advantage IRMS (Thermo
281 Scientific) with a ConFlow IV (Thermo Scientific). Samples were injected with a TriPlusRSH autosampler to
282 a split/splitless injector operated in splitless mode at 280 °C. The oven was equipped with an InertCap
283 5MS/NP column (0.25 mm x 30 m x 0.25 μm) (GL Sciences, Japan) and was heated from 80 to 215°C at 15°C
284 $min^{-1}$, then to 320°C at 5°C $min^{-1}$, and then held at 320°C for 10 minutes. Column effluent was combusted at
285 1020 °C.
286
287 Raw isotope ratios were converted to the VPDB scale using Thermo Isodat 3.0 software and pulses of
288 reference gas at the beginning and end of each analysis. The sample $\delta^{13}C$ values were further corrected using
289 the linear regression of measured and known values for a standard mix of *n*-alkanes (*n*-$C_{17, 19, 21, 23, 25, 28, 34}$) of
290 known isotopic composition (provided by Arndt Schimmelmann, Indiana University), which was run at
291 varying concentrations at the beginning and end of each sequence, as well as after every 6-8 injections of
292 samples. This standard was also used to monitor for instrumental drift and for any isotope effects associated
293 with retention time or peak size. The average standard deviation for these standards during the analysis period
294 was 0.6 ‰ ($n$ = 182)**,** and their average offset from known values was -0.1 ‰. An additional quality control
295 standard of *n*-$C_{29}$-alkane was analyzed at least three times per sequence, and had a standard deviation of 0.18
296 ‰ ($n$ = 15) during the analysis period. FAME $\delta^{13}C$ values were corrected for the carbon added during
297 methylation by isotopic mass balance, and reported errors represent propagated errors from the replicate
298 measurements and from the uncertainty associated with the added carbon, which was determined by
299 methylating and analyzing phthalic acid of known isotopic composition (provided by Arndt Schimmelmann,
300 Indiana University).
301
302 ***3. Interpretative Framework and Results***
303 *3.1. Palynological indications for vegetation dynamics and land-use in the catchment*
304 The relative abundances of the tree, shrub and herb pollen, microscopic charcoal influx (particles/$cm^2$/y), as
305 well as cultural indicators such as *Cerealia* type and *Plantago lanceolata* (ribwort plantain) pollen, and spores

306 from coprophilous fungi have proven to be robust indicators for evaluating land-use dynamics and vegetation
307 change (see Tinner et al. (2003) for further information). We focused on these proxies to reconstruct the
308 history of agriculture and divided the pollen record into three local pollen zones (PMUR-1-3) in order to
309 assess statistically significant vegetation changes (Fig. 3, appendix B).
310
311 The sediment record reaches back to approximately 5800 BCE, which falls into the Late Mesolithic Period
312 (start of PMUR-1). There is no archaeological evidence of human settlements in the Swiss Plateau region at
313 that time (UNESCO Palafittes, 2015). During PMUR-1, a dominance of pollen of temperate trees and shrubs
314 such as *Ulmus, Quercus, Tilia, Acer, Fraxinus, Corylus* and *Hedera helix* and monolete fern spores were
315 present, suggesting that mixed oak forests (Quercetum mixtum) dominated the region around Lake Murten
316 (ca. 70% tree pollen during the Neolithic Period, Fig. 3). At the same time pollen of *Abies* and *Fagus* reached
317 their empirical limit, suggesting that these trees expanded locally (Birks and Tinner, 2016). *Fagus sylvatica*
318 (beech) and *Abies alba* (silver fir) are both shade-tolerant mesophilous late-successional trees species. The
319 shift to mixed beech forests was found throughout the entire Swiss Plateau during the Neolithic Period. At
320 Lake Murten, a representative site for the western part of the Swiss Plateau close to the Jura Mountains, *Fagus*
321 *sylvatica* was co-dominant with *Quercus* (Ammann, 1989; Hadorn, 1992; Richoz and Haas, 1995).
322
323 During the Neolithic Period of the core, the charcoal influx increased to 6500 particles/cm$^2$/y ($n$ = 14),
324 indicative of moderate fire activity in the region. Generally, the fire history is similar to the temporally high
325 resolution charcoal results from nearby Lake Lobsigen (ca. 20 km away, Tinner et al., 2005). After ca. 4500
326 BCE, fire sensitive taxa such as *Ulmus, Tilia, Fraxinus, Acer* and *Hedera helix* decreased, while pollen of
327 pioneer species such as *Betula, Corylus avellana* and *Salix* and heliophilous *Juniperus* shrubs increased.
328 These results are consistent with the overall slash and burn agricultural practices of the Neolithic Period.
329 *Plantago lanceolata* pollen and *Sporormiella* spores were scattered throughout this sedimentary interval, but
330 at concentrations that are suggestive of low levels of human activity during the Neolithic Period (Fig. 3).
331
332 Towards the end of the Neolithic Period (2540 BCE; Figure 3), the first pollen occurrence of Cerealia type (t.)
333 was detected, revealing a probable human activity and field cultivation in particular. Around 2200 BCE, the

cultural period of the early Bronze Age started. However, no crucial vegetation change is visible in the overview pollen diagram from this time (Figure 3). The only indication of further human influence is a slight rise in charcoal influx coupled with an increase of pollen from more disruption-resistant *Fagus* and *Urtica*.

Starting towards the end of the Late Bronze Age period (ca. 1100 BCE, PMUR-2), crucial changes in the vegetation around the lake were observed, roughly coincident with the onset of the Iron Age cultural period (800 - 20 BCE). We observed a slow but significant decrease in tree pollen percentages, down to 30% (650 CE, Figure 3). In the course of this forest decline, *Fagus* and *Abies* pollen in particular decreased substantially. Furthermore, a notable peak in the charcoal influx of 14'360 particles/cm$^2$/y occurred around 430 BCE (Figure 3). This so called Iron Age-peak in charcoal influx has also been observed at other sites in the Swiss Plateau and south of the Alps (Tinner et al., 2003). The timing of deforestation seems to correlate not only with the elevated charcoal influx, but also with the beginning of a continuous curve in the cultural indicator proxies, such as Cerealia t., *Plantago lanceolata* or Poaceae pollen (Figure 3). As Cerealia t. pollen are dispersed locally and do not reach large distances (Soepboer et al., 2007; Tinner et al., 2003), these results suggest cereal fields were in close proximity to Lake Murten. The agricultural intensification during the Late Iron Age to Roman Period was accompanied by a substantial expansion of meadow and ruderal species such as *Artemisia*, Cichorioideae, *Ranunculus acris* t. and *Rumex acetosa* t. A similar development has also been observed in pollen records from other sites in the Swiss Plateau, such as Lake Lobsigen (Ammann, 1989). During the Iron Age, dung-spores (*Sporormiella*, Fig. 3) rose continuously and remained elevated throughout the Roman Period, where a temporal maximum of 1.4% at 350 CE was identified. Cerealia t. pollen percentages also increased steadily during the Roman Period (20 BCE to 5$^{th}$ century CE, Fig. 3). Furthermore, the Roman Period stands out clearly in the pollen record and is characterized by the introduction of new crops such as *Castanea sativa*, *Juglans regia* and *Secale cereale*.

The last local pollen zone PMUR-3 started ca. 380 CE and was characterized by further deforestation (until 650 CE, 30% tree pollen), mostly at the expense of *Abies* and *Fagus*. Following the deforestation peak (650 CE), tree pollen percentages increased again to 40-50%, mainly due to the increase of *Quercus* pollen percentages (Fig. 3). From the Medieval Period to the 19$^{th}$ century, oak stands provided an important

362 livelihood in Switzerland, consistent with our findings. Cereal cultivation (Cerealia t.; *Secale cereale*) was
363 also prevalent during this time. Herb pollen percentages of cultural meadow and ruderal taxa such as *Plantago*
364 *lanceolata*, Poaceae, *Urtica*, *Artemisia, Trifolium pratense* t., etc. were present at a continuously high level,
365 indicating ongoing land-use in the nearby catchment area until today. The afforestation trend was
366 accompanied by a simultaneous increase in the shrubs *Juniperus* and *Salix* but also slight increases in *Calluna*
367 and Ericaceae pollen. The heathland components commonly grow on open patches at rather nutrient-poor and
368 extensive meadows.
369
370
371 **Figure 3:** Palynological indications for past land-use around Lake Murten, Switzerland. A. Abundance of
372 Cerealia type (including *Secale cereale*) and *Plantago lanceolata* pollen as well as *Sporormiella* spores. B.
373 Charcoal influx. C. Normalized abundance of tree, shrub and herb pollen, as well as the subdivision into
374 significant local pollen zones 1-3. The thick lines in A and B represent trends derived from a locally weighted
375 scatterplot smoothing (LOESS, span = 0.3, n = 80). Abbreviations: Mesolithic Period (MP), Roman Period
376 (R), Modern Times (MT).
377
378 *3.2. Sedimentary leaf wax distributions*
379 The range and relative molecular abundances of sedimentary leaf waxes have been widely used to trace
380 environmental changes (Bush and McInerney, 2013). Leaf waxes are produced to coat the vascular leaf
381 surface, and serve as an outer protection against the environment (Eglinton and Hamilton, 1967). Their
382 molecular components, such as long-chained *n*-alkanes or *n*-carboxylic acids, have a refractory structure and
383 are well preserved in the environment over geological time scales (Eglinton and Eglinton, 2008).
384 A common ratio to describe leaf wax distribution patterns is the average chain-length (ACL) of *n*-alkanes or
385 *n*-carboxylic acids (Bush and McInerney, 2013) (Formula in appendix C). For sediments it has been proposed
386 that the ACL of *n*-alkanes is a broad indicator of shifts in the catchment's plant community. A predominance
387 of relatively long-chained *n*-alkanes (or *n*-carboxylic acids) is typical for leaf waxes originating from higher
388 terrestrial plants (Eglinton and Hamilton, 1967). In contrast, *n*-alkanes from more aquatic sources, such as

389 microalgae or macrophytes, typically have relatively high abundances of middle and short-chained
390 homologues (Ficken et al., 2000; Sachse et al., 2004).
391
392 In the sedimentary record of Lake Murten, ACL values of *n*-alkanes varied between 27.8 and 28.9 with a
393 mean of 28.4 ($n$ = 71, Figure 4). *n*-$C_{29}$ alkane was the most abundant homologue. The predominance of
394 relatively long-chained *n*-alkanes in the record indicates contributions of terrestrial leaf waxes sourced from
395 higher plants. ACL trends from Lake Murten sediment (Figure 4) are correlated with arboreal pollen
396 abundances (Figure 3), supporting the assumption that the leaf waxes are predominantly of terrestrial plant
397 origin.
398
399 The carbon preference index (CPI) measures the abundance of odd-numbered relative to even-numbered
400 *n*-alkane chain-lengths (Formula in appendix C). High CPI values (>1) are characteristic for most modern
401 plants (Bush and McInerney, 2013). Hence, in a sedimentary sequence CPI can provide an information on
402 whether the *n*-alkanes are likely derived from a plant source, or whether they have been subject to significant
403 microbial degradation or petrogenic inputs, both of which are associated with lower CPI values and greater
404 relative contributions from even-numbered *n*-alkane homologues (Haas et al., 2017; Tao et al., 2015).
405
406 The *n*-alkane distributions from the sediments of Lake Murten had CPI values ranging from 4.3 to 9.4 with a
407 mean of 7.2, demonstrating a strong dominance of odd-numbered *n*-alkanes (appendix C). We thus conclude
408 that fossil leaf wax contribution from bedrock and microbial degradation seem to be minimal and that the leaf
409 waxes are well preserved in the sediments.
410
411 The ACL and CPI values of sedimentary *n*-carboxylic acid distributions also support the conclusion that leaf
412 waxes in Lake Murten are predominantly sourced from terrestrial leaf waxes (summarized leaf wax data is
413 given in appendix C). However, *n*-carboxylic acid and *n*-alkane distributions are highly variable within
414 different plant groups, species and even the plant itself and can be influenced by various environmental
415 factors, such as temperature and relative humidity (Bush and McInerney, 2013). Furthermore, the original
416 (terrestrial) leaf wax signal can be diluted during transport, deposition or degradation by addition of

compounds of other sources (Bush and McInerney, 2013). This problem of source control can be mitigated by using a compound-specific approach, focusing only on compound fractions of relatively known terrestrial origin.

### *3.3. $\delta^{13}C$ isotopic composition of sedimentary leaf waxes*

The carbon isotopic composition of specific long-chained leaf waxes can be useful for inferring relative leaf wax sources (Diefendorf and Freimuth, 2017). Plant physiology, carbon fixation mechanisms (which differ for $C_3$ and $C_4$ plants) and environmental factors such as relative humidity and temperature are responsible for pronounced differences in the $\delta^{13}C$ signature of plant OM (Farquhar et al., 1982). Analyzing $\delta^{13}C$ values of specific leaf wax compounds in sediment allows relative inputs from various OM sources to be discriminated (Rieley et al., 1991).

In Lake Murten, the $\delta^{13}C$ values of sedimentary long-chained leaf waxes ($\delta^{13}C_{lw}$), including the *n*-$C_{28}$, *n*-$C_{30}$, *n*-$C_{32}$ carboxylic acids and *n*-$C_{29}$ and *n*-$C_{31}$ alkanes, ranged from -32.9 to -37.3‰ with a mean value of -34.6‰ ($n = 41$) (Figure 4). They were depleted by approximately 4‰ relative to the bulk sedimentary isotopic composition ($\delta^{13}C_{bulk}$) measured by Haas et al. (2019), which ranged from -28.2 to -32.0‰ with a mean value of -30.1‰ ($n = 62$). The $\delta^{13}C$ values of shorter homologues such as *n*-$C_{21}$ alkanes or *n*-$C_{20}$ carboxylic acids were in the same range as their longer chained counterparts (appendix D). The relatively depleted carbon isotopic composition is consistent with the $\delta^{13}C$ signature of higher terrestrial plants following the $C_3$ pathway for carbon fixation (Mays et al., 2017; Rieley et al., 1991). This assumption is supported by relatively high ACL and CPI values for both *n*-alkanes and *n*-carboxylic acids. Since the $\delta^{13}C$ values of long- and short-chained *n*-alkanes and *n*-carboxylic acids differed only slightly relative to each other, we assume a similar terrestrial leaf wax source for all these compounds. The offset of approximately 4‰ between $\delta^{13}C_{bulk}$ and $\delta^{13}C_{lw}$ values is attributed to the biosynthetic depletion of leaf waxes relative to the carbon isotopic composition of the bulk plant tissue (Collister et al., 1994). Differences between $\delta^{13}C_{bulk}$ and $\delta^{13}C_{lw}$ values can also occur if the sedimentary OM incorporates isotopically-enriched OM from autochthonous sources such as algae (Rieley et al., 1991). This possibility is unlikely in Lake Murten given the elevated ACL values and the relatively depleted $\delta^{13}C$ values of the short-chained *n*-carboxylic acids.

445

446 The evaluation of simultaneous changes among different compound-specific $\delta^{13}C$ signatures is an additional
447 approach to interpret changes in the sedimentary leaf wax sources (Diefendorf et al., 2010; Yamamoto et al.,
448 2010). The $\Delta\delta^{13}C$ offset (‰) represents the difference between specific long- and short-chained leaf wax $\delta^{13}C$
449 values (Figure 4). In Lake Murten, the $\Delta\delta^{13}C$ offset between *n*-$C_{32}$ and *n*-$C_{28}$ carboxylic acids ($\Delta\delta^{13}C_{32\text{-}28}$)
450 showed the largest variations and seemed to react more sensitively to leaf wax source changes, compared to
451 $\Delta\delta^{13}C_{32\text{-}30}$ and $\Delta\delta^{13}C_{30\text{-}28}$ (Figure 4). During most parts of the Neolithic Period and the Bronze Age, $\Delta\delta^{13}C_{32\text{-}28}$
452 values were positive, with the longer homologue typically ~2‰ enriched relative to the shorter one. Starting
453 with the Iron Age, however, $\Delta\delta^{13}C_{32\text{-}28}$ decreased steadily and reached negative values during the Roman and
454 the Medieval Period, indicating that *n*-$C_{28}$ carboxylic acid became relatively $^{13}C$-enriched relative to *n*-$C_{32}$
455 carboxylic acid. The overall decrease in $\Delta\delta^{13}C$ from the Late Iron Age to the Medieval Period (Figure 4) is
456 coeval with a decrease in the abundance of trees in the catchment (Figure 3).

457

458 One possible explanation is that during most parts of the Neolithic Period and the Bronze Age, a greater
459 proportion of the *n*-$C_{28}$ carboxylic acids were sourced from trees, which on average have leaf waxes with
460 lower $\delta^{13}C$ values than do non-woody $C_3$ plants (Diefendorf and Freimuth, 2017; Magill et al., 2013). With
461 ongoing deforestation, relatively more of the sedimentary *n*-$C_{28}$ carboxylic acid would have been sourced
462 from non-woody C3 plants, making it more enriched than before and thus lowering the $\Delta\delta^{13}C_{32\text{-}28}$ during
463 phases of land-clearing. This interpretation is supported by the overall variability in ACL and the arboreal
464 pollen abundances.

465

466 Enhanced primary production in Lake Murten could also explain the negative shift in $\Delta\delta^{13}C_{32\text{-}28}$ values that
467 began in the Late Iron Age and continued into the second half of the Medieval Period. *n*-Carboxylic acids
468 produced by algae are relatively enriched in $\delta^{13}C$ compared to terrestrial sources, and *n*-$C_{28}$ carboxylic acids
469 can be produced by microalgae (van Bree et al., 2018; Volkman et al., 1980). Increased primary productivity
470 within the lake could therefore also lower $\Delta\delta^{13}C_{32\text{-}28}$ values by increasing the $\delta^{13}C$ values of *n*-$C_{28}$ carboxylic
471 acids. However, clear evidence of enhanced primary production and eutrophic conditions that led to varve
472 formation have only been observed during the Late Iron Age to Early Roman Period (200 BCE - 50 CE, with

the updated age-model, Haas et al., 2019). We assume that increased contributions of *n*-$C_{28}$ carboxylic acids from microalgae would only be relevant for these documented periods of hypoxia. Furthermore, if decreases in the $\Delta\delta^{13}C_{32\text{-}28}$ offset were caused by enhanced algal productivity, we would expect them to correspond to a decrease in the *n*-carboxylic acid ACL, which was not the case.

### *3.4. Relative ages of sedimentary leaf wax compounds*

In addition to the complications stemming from multiple sources for specific leaf wax compounds, their relative ages might also vary depending on the time needed for the cascade from synthesis to primary deposition in soils, to transport and finally to re-deposition in sediments (Douglas et al., 2014). Compound-specific radiocarbon dating (CSRA) allows the mean transit time of leaf waxes ($MTT_{lw}$) between plant synthesis and deposition in the sedimentary environment to be estimated (Douglas et al., 2018). Relative changes in $MTT_{lw}$ are closely associated with soil processes that can influence the recalcitrant "deep" SOC pool (Douglas et al., 2018; Feng et al., 2013; Smittenberg et al., 2006). It has been proposed that pre-aged leaf waxes, as part of the recalcitrant SOC pool, are introduced into the carbon cycle during phases of land-use, when the structure of top- and subsoil gets disturbed (Butman et al., 2015; Douglas et al., 2018; Lal, 2002). In a sedimentary archive, periods of human land-use may thus be recorded in terms of increasing age-offsets (i.e. $MTT_{lw}$) between individual long-chained leaf waxes and the corresponding deposition age (Douglas et al., 2014; Gierga et al., 2016). This has the advantage that the influence of a potential hard water effect can be limited substantially compared to analyses on the heterogenous bulk sedimentary OC due to better source control (Gierga et al., 2016). The predominance of relatively long-chained *n*-alkanes (or *n*-carboxylic acids) in the sediments of Lake Murten is characteristic for leaf waxes originating from higher terrestrial plants (increased ACL, Eglinton and Hamilton, 1967). The ACL even increased with ongoing land use during the Roman agricultural period, suggesting that the increased age-offsets are unlikely to be due to an increase of aquatic plant material which might have radiocarbon ages affected by hard water. Additional evidence that the leaf wax age-offsets are unlikely to be caused by aquatic plant inputs comes from the relatively depleted $\delta^{13}C$ values of these compounds ($\delta^{13}C$ from -32.9 to -37.3‰). These are consistent with a C3 terrestrial plant origin, as aquatic plants tend to be somewhat more enriched in $^{13}C$ (Fry and Sherr, 1984). In Lake Murten, we thus interpret increases in $MTT_{lw}$ as an indicator of enhanced input of soil-derived and pre-aged leaf waxes,

501 corresponding to periods of increased soil erosion. Decreasing $MTT_{lw}$, on the contrary, is interpreted as a sign
502 of soil stabilization.
503
504 Compound-specific $^{14}C$ dating of long-chained *n*-alkanes as well as bulk *n*-alkane fractions revealed that mean
505 ages of leaf waxes in Lake Murten sediments are hundreds of years older than the estimated deposition age of
506 the surrounding sediment. On average the $MTT_{lw}$ ranged from -600 to 4850 years with a mean of 450 years
507 (Figure 4). Due to low sample masses and the applied contamination corrections (appendix E) the errors of the
508 *n*-alkane $^{14}C$ ages were relatively large (approximately 700 y, $n = 32$). Compound-specific *n*-alkane samples
509 with masses below 20 µg carbon had the highest errors. In three cases (50, 1110 and 1900 CE) we were able
510 to date two different fractions from the same bulk *n*-alkane sample. In all cases the ages of the different chain-
511 length fractions differed significantly by several hundred years. However, we assume that this effect was
512 caused by the strong sample mass dependency of radiocarbon dating of small samples rather than a primary
513 environmental signal (Hanke et al., 2017). Most of the reported ages that seem too young (e.g. all $n\text{-}C_{31+33+35}$
514 alkane fractions, Figure 4) were measured on samples with a relatively low carbon content (ca. 12 µg C, $n =$
515 3). The effect of mass dependency was also visible when comparing the ages and errors of compound-specific
516 fractions (all < 20 µg C) and bulk *n*-alkane fractions (all > 20 µg C). Certain measurement artifacts could be
517 countered by applying a locally weighted scatter-plot smoothing function (LOESS) including both compound-
518 specific and bulk fractions. This smoothing function includes the assumption of a similar leaf wax source for
519 short and long-chained homologues in the sediments of Lake Murten, which is supported by compound-
520 specific $\delta^{13}C$ measurements and the sedimentary leaf wax distributions (more details can be found in appendix
521 C). Due to the relatively large errors in the CSRA data, not all changes in $MTT_{lw}$ are significant. For this
522 reason we only describe broad trends in the $MTT_{lw}$ data and compare it to $MTT_{OC}$, which has much smaller
523 errors.
524
525
526 ***Figure 4:*** A. Average chain length of *n*-alkanes $n\text{-}C_{23\text{-}33}$ (ACL) from sediments of Lake Murten, Switzerland.
527 B. $\delta^{13}C$ composition of leaf waxes. C. $\Delta\delta^{13}C$ offset. D. Mean transit time of different *n*-alkane fractions

528 ($MTT_{lw}$) and bulk sediment ($MTT_{OC}$). The thick lines represent trends derived from LOESS (span ~ 0.3, n =
529 80). Abbreviations: Mesolithic Period (MP), Roman Period (R), Modern Times (MT).
530
531 ***4. Discussion: History of land use in the Lake Murten catchment***
532 The first signs of human activity in the catchment area of Lake Murten appeared during the Neolithic Period,
533 when several pile dweller communities occupied the lake shore (UNESCO Palafittes, 2015). In the Alpine
534 region, early pastoral activity and slash and burn practices to gain arable land during this time are indicated by
535 elevated charcoal influx, as well as the first occurrences of *Sporormiella* spores and *Plantago lanceolata*
536 pollen (Dietre et al., 2017; Schwörer et al., 2014; Tinner et al., 2003; Wehrli et al., 2007). Although there is
537 evidence of human activity around Lake Murten during this interval, no significant changes were observed in
538 the sedimentary leaf wax distribution (ACL) and the overall $\delta^{13}C_{lw}$ isotopic composition (Figure 4). The
539 $MTT_{lw}$ trend, on the other hand, indicates increased input of pre-aged leaf waxes from 5200 to 3400 BCE ($n$ =
540 3). Also, $MTT_{OC}$ values suggest that input of pre-aged organic carbon increased during the same interval.
541 Early human activity might be responsible for the excursions in $MTT_{lw}$ and $MTT_{OC}$ values. An alternative
542 explanation comes from the lithological succession of the core. The early interval with elevated $MTT_{lw}$ and
543 $MTT_{OC}$ values is mostly part of Unit 5 (5600 - 3700 BCE), which is composed of sediments with high detrital
544 element concentrations (Haas et al., 2019). This suggests either a new source of sediments, which could be
545 due to naturally occurring river diversions, or a climatically caused increase in soil erosion corresponding to
546 wetter climate conditions as suggested by Magny (2004).
547
548 Unit 5 (957 - 766 cm) was deposited during a reported lake level high-stand for 26 lakes in Western
549 Switzerland and France that occurred in the period of 4400 - 3950 BCE (Magny, 2004). In the Swiss lowlands
550 phases of higher lake-level were triggered by enhanced annual precipitation and lower summer temperatures
551 (Magny, 2004), leading to an outwash of detritus and probably soil material, including pre-aged leaf waxes.
552 The age-depth model was updated substantially compared to the model in Haas et al. (2019). As a result, the
553 progression of the age-depth model during the Neolithic Period is rather uncertain (Figure 2, Unit 5, 957 - 766
554 cm) and the variable MTT values are strongly dependent on the age-depth model. The largest confidence
555 intervals (95%) for the age-depth model occurred during Unit 5 (ca. 500 years, Figure 2) due to two

radiocarbon dates that lie slightly outside the curve (Figure 2). If the model would be changed so that it would pass through these points more clearly, the corresponding deposition ages would have been older and thus the $MTT_{lw}$ and $MTT_{OC}$ values during Unit 5 much smaller. As a consequence, the errors in this part of the core would have been unrealistically small, which is why this version of the model was omitted (See appendix A for the alternative age-depth model).

All data in the lower part of the core until ca. 3700 BCE should be interpreted with caution. There are indications that the last two data points in the age-depth model could also be classified as uncertain due to a biostratigraphic event, namely the rise of *Abies alba* and *Fagus sylvatica* around 6000 BCE, that was observed in other palynological publications near the study area (Tinner et al., 2018). In the sediments of Lake Murten the first rise of *Abies alba* (above 2%) occurred slightly earlier approximately 5000 – 5500 BCE (see appendix B). This could imply that the deposition ages of the lowermost sediments could also be older by ca. 500 – 1000 years, and that the age-model rather shows a minimum age (see also appendix A for an alternative age-depth model). However, the resolution of the palynological analysis would need to be increased substantially in order to verify this assumption. After 3700 BCE, the age-depth model is relatively stable until today (Figure 2) and more accurate statements about environmental changes in the catchment can be made.

Towards the transition into the Bronze Age, around 2500 BCE, increasing *Sporormiella*, *Plantago lanceolata* percentages and also the first occurrence of Cerealia t. pollen were documented (Figure 3), demonstrating that human activity including cattle raising and arable farming in close proximity to the lake shore were increasing. This result is also in close agreement with archaeological evidence. Numerous pile dwelling remains from the Neolithic Period were found in and around Lake Murten and dated using dendrochronology (Schibler and Jacomet, 2010). The interval of increased human activity (ca. 3000 - 2000 BCE) in the Lake Murten sedimentary record corresponds well with the reported ages of pile dwellings excavated in Faug, Vallamand and Muntelier (Figure 1, UNESCO Palafittes, 2015).

Despite new innovations in agricultural field cultivation (as indicated by Cerealia t. pollen), no significant changes in the leaf wax distributions and $\delta^{13}C_{lw}$ signature could be detected at this time (Figure 4). Only the $MTT_{lw}$ gradually decreased, whereas no changes in the bulk sediment age offset were visible during this

584 period. Based on the long-lasting decrease in $MTT_{lw}$ and the disagreement with land-use indicators, we
585 assume climatic controls were more important than anthropogenic controls on the leaf wax transit time during
586 this period. Magny (2004) also suggested that warmer and dryer climatic conditions prevailed during this
587 period (ca. 2500 BCE), favoring wheat production. Decreased precipitation might naturally lower the outwash
588 of SOC and pre-aged leaf waxes without changing their distributions or $\delta^{13}C$ values.
589
590 During the Bronze Age, from 2200 - 800 BCE, land-use indicators remained low, even though nine
591 archaeological sites of pile dwellings are known from this time (Figure 1, UNESCO Palafittes, 2015). The
592 only signs of land-clearing were a minor increase in the charcoal influx and decrease in tree pollen
593 percentages in the Early Bronze Age (1500 BCE). This timing also roughly correlates with one elevated
594 $MTT_{lw}$ value, suggesting a short period of soil erosion. However, a higher sample resolution would be needed
595 to confirm that land-clearing and shorter periods of soil erosion existed during this interval.
596
597 During the Iron Age, 800 - 15 BCE, tree percentages started to decrease steadily and the charcoal influx rose
598 to a distinct peak, ca. 430 BCE, indicating severe land clearing (Figure 3). The interval of deforestation during
599 the La Tène cultural period (Late Iron Age) to the Early Roman Period was also accompanied by sharp
600 increases in *Sporormiella*, *Plantago lanceolata* and Cerealia t. percentages, indicating the beginning of large-
601 scale farming with cattle raising and field cultivation in the region (Figure 3). The earlier increase in
602 *Sporormiella* spores might suggest that pastoralism was dominant during the Late Iron Age. This past land-
603 use period corresponds nicely with the increases in sediment mass accumulation rate and detrital input
604 documented in our previous study (Haas et al., 2019).
605
606 Evidently, land-use and deforestation also had an influence on the leaf wax composition. With the onset of the
607 Late Iron Age, ACL increased significantly to a temporal maximum of 28.8 at 140 BCE (Figure 4). At the
608 same time, $\Delta\delta^{13}C$ offsets started to decrease steadily, suggesting a change in the leaf wax source towards open
609 grasslands. $MTT_{lw}$ and $MTT_{OC}$ trends increased simultaneously during the Iron Age, consistent with the
610 growing influence of agriculture on soil erosion.
611

612 The deforestation trend continued with the onset of the Roman Period, reflecting the high demand for wood
613 and arable land that was needed for the newly founded Roman city *Aventicum* and its 20'000 inhabitants, at
614 the southern shore of Lake Murten (Castella et al., 2015) (Figure 1). Increased land-use indicators such as
615 *Sporormiella*, *Plantago lanceolata* and Cerealia t. point towards large-scale farming and the extension of
616 human pressure on the environment.
617
618 In the leaf wax record, the Roman Period was accompanied by relatively high but decreasing ACL (from 28.4
619 to 28.0, 70 BCE – 280 CE) and a slight decrease towards more $^{13}$C-depleted values for the leaf waxes (Figure
620 4). The $\Delta\delta^{13}C$ offset increased slightly despite the overall downward trend, due to a pulse of $^{13}$C-depleted *n*-
621 $C_{28}$ carboxylic acids. This effect might originate from the affiliation of leaf waxes with soil aggregates.
622 Mineral matrix protection of leaf waxes could have served as an effective protection from microbial
623 degradation or re-synthesis, which leads to a relative enrichment in $\delta^{13}C$ (Douglas et al., 2018; Matsumoto et
624 al., 2007; Vonk et al., 2010). The elevated CPI of about 9 at 110 CE (appendix D) would support the
625 assumption that less microbially influenced leaf wax material affiliated with soil aggregates was washed into
626 the lake during this time.
627
628 Correlating with the onset of Late Iron Age to Early Roman land-use, soil erosion indicators drastically
629 increased, consistent with our previous study (Haas et al., 2019). The mean transit time of bulk sedimentary
630 OC ($MTT_{OC}$ of 1500 years) peaked at 170 BCE with the updated age-model, revealing terrestrial runoff of
631 pre-aged SOC due to human induced soil erosion. In the leaf wax record, a similar peak was detected in the
632 transit time ($MTT_{lw}$ of around 700 years from 70 BCE to 150 CE), supporting the hypothesis of Early Roman
633 soil degradation in the catchment (Figure 4). There was minimal time-lag of around 100 years between the
634 $MTT_{lw}$ and $MTT_{OC}$ maxima. This might be a source effect of the two different organic fractions. Sedimentary
635 OM has a very heterogeneous composition, containing OC of various allochthonous and autochthonous
636 sources of different origin and ages (Gierga et al., 2016). Additionally, bulk sediment $^{14}$C data is prone to so
637 called "hardwater effects", depending on the bedrock composition of the catchment. Due to the dissolution of
638 limestone, algae and aquatic plants incorporate dissolved inorganic carbon (DIC) that is considered
639 radiocarbon dead, which may lead to a dilution of the bulk sediment $^{14}$C-concentration (Fowler et al., 1986).

640 The sedimentary leaf waxes, on the contrary, are predominantly of terrestrial instead of aquatic origin and
641 offer a better source control. We thus posit that the $MTT_{lw}$ maximum during the Early Roman Period was
642 mainly the result of anthropogenic soil erosion.
643
644 The input of pre-aged leaf waxes might have an effect on common ratios such as ACL, CPI and $\delta^{13}C_{lw}$ records
645 (Douglas et al., 2014). Due to the time lag between synthesis and sedimentary deposition, the environmental
646 signals might be delayed by the transit time of the individual compounds. In the Lake Murten setting,
647 however, this effect appears to be restricted to the periods of land-use. During times of land-use and enhanced
648 soil input we detected rising ACL, $\Delta\delta^{13}C$ offsets and $MTT_{lw}$ but decreasing $\delta^{13}C_{lw}$ values (Figure 4). The
649 described excursions correspond well with the palynologically derived land-use periods and do not show
650 significant time lags, suggesting that only a smaller portion of the long-chained leaf waxes were pre-aged.
651 During undisturbed times, the sedimentary leaf wax distribution (ACL and $\Delta\delta^{13}C$ offsets) seems to have been
652 controlled by vegetation and the ecological changes inferred from the independent pollen record (Figure 3).
653
654 After the fall of the Roman Empire, during the Early Medieval Period, land-use indicators such as the charcoal
655 influx as well as *Sporormiella* or *Plantago lanceolata* percentages decreased (ca. 650 CE). At this point the
656 forest around Lake Murten had been decimated to ca. 20% of its initial extent. Historically, these sediments
657 were deposited during the Great Migration Period (ca. $4^{th}$ to $6^{th}$ century CE), which is poorly represented in
658 archaeological findings (Nast, 2006). Tinner et al. (2003) documented a reduction of agricultural activities
659 around the 6th century CE accompanied by a short period of renaturation in three Swiss lakes. In the Lake
660 Murten pollen record, afforestation was also identified, but several hundred years later, ca. 700 CE (Figure 3).
661 The timing discrepancy can either be assigned to the low sample resolution, an inaccurate age-depth relation,
662 and/or to regional differences in population discontinuities in Switzerland.
663
664 In the leaf wax record a minimum in the ACL trend occurred (ACL of ca. 28.2, 350 CE), which might be
665 indicative of a slight renaturation and forest regrowth during this period (Figure 4). This agrees with the
666 $MTT_{lw}$ values, which steadily decreased and reached a temporal minimum of -340 years at 390 CE, suggesting
667 soil stabilization due to vegetation regrowth. A similar trend in the $MTT_{OC}$ was observed. Since *Aventicum*

668 most likely had its largest population in the first two centuries CE, approximately 200 - 300 years of soil
669 stabilization was needed to reach $MTT_{lw}$ values similar to those before the great land-clearing episode.
670
671 After 1000 CE, the tree pollen percentages decreased slightly, probably marking the growing influence of
672 Medieval agriculture in the region (Figure 3). Charcoal influxes, however, remained at a relatively low level
673 (around 7100 particles/$cm^2$/ y), which might indicate that less effort was needed to re-open the shrub-
674 dominated lands compared to the Late Iron Age to Early Roman Period. Palynological indicators, such as
675 Cerealia t. and *Plantago lanceolata* pollen and *Sporormiella* spores, were present in approximately the same
676 range as in the Roman Period, demonstrating active Medieval land-use in the catchment. The observed
677 changes also agree with historical developments. The Burgundians built the Early Medieval fortress of Murten
678 in 814 CE on a pre-existing village back from Celtic to Roman times (documented as *Muratum*, 515 CE)
679 (Schöpfer, 2016).
680
681 In the leaf wax record, Medieval land-use was only partly recorded. ACL rose to relatively high values (>28.5,
682 1000 CE) starting in the second half of the Medieval Period, probably indicating elevated input of leaf waxes
683 of terrestrial origin (Figure 4). Around the same time, $MTT_{lw}$ rose to 1900 years (900 CE), reaching a
684 temporal maximum. In the $MTT_{OC}$ no temporal maximum was detected but rather a steady increase (Haas et
685 al., 2019). This agrees with the results of our previous study, where we documented elevated detrital input
686 during the Medieval Period (Haas et al., 2019). Building on previous argumentation we thus assume that an
687 increase of human-induced soil erosion was responsible for this aging-effect in the sedimentary leaf-wax
688 record.
689
690 Around 1830 CE, the charcoal influx increased again and tree pollen percentages reached another minimum,
691 revealing a short period of deforestation during the course of the industrialization (Figure 3). Cultural
692 indicators such as *Plantago lanceolata*, and new indicators, e.g. *Platanus*, *Zea mays*, and *Carum carvi*,
693 increased significantly, suggesting high human activity in the catchment. This last development agrees with
694 the mechanization of agriculture, drainage of swamps and several water level corrections that accompanied
695 the intensification of agriculture in the region around the lake (Nast, 2006).

696

697 The effect of land-use on the leaf wax composition is more pronounced during the Industrial Period compared
698 to the Roman or Medieval land-use periods (Figure 4). Simultaneous changes in the $\delta^{13}C$ values of leaf wax
699 compounds, towards more depleted values, and the steep increase in $MTT_{lw}$ (Maximum of 4850 years, 1950
700 CE) show that soil erosion increased substantially. New agricultural innovations, including mechanization,
701 allowed deeper plowing and most likely led to a more efficient mobilization of the deep SOC pool.
702 Furthermore, the large-scale water corrections that were applied during this time contributed to declining lake
703 surface levels and to the draining of the large swamp areas north of the lake to make new land for agriculture
704 available. Therefore, destabilization of the peatlands, leading to soil subsidence and erosion, might also be
705 responsible for the recent increase in $MTT_{lw}$.

706

707 ***5. Conclusions***

708 A detailed reconstruction of the land-use history and its long-term impact on the environment in the Swiss
709 Plateau was produced through a combination of lake sediment pollen, spore, non-pollen palynomorphs and
710 microscopic charcoal analysis, as well as the evaluation of the distribution, carbon isotopic composition and
711 the relative ages of sedimentary leaf waxes in Lake Murten. Although pile dweller communities of the
712 Neolithic Period and the Bronze Age left their traces in the sedimentary record (low level slash and burn
713 agriculture, first cultural indicators for human activity), their influence on the local environment seems to have
714 been minimal. Based on a comparison of the relative input of soil-derived leaf waxes and independent lake
715 level reconstructions, we conclude that soil erosion during the Neolithic Period and the Bronze Age was
716 mostly driven by precipitation.

717

718 With the onset of the Late Iron Age and the rise of the La Tène culture, human activities had a greater impact
719 on soil erosion in Lake Murten's catchment. At the beginning of the Iron Age (ca. 800 BCE), continuous
720 deforestation was initiated, including severe slash and burn practices around 400 BCE (Figure 3). Cultural
721 indicators increased distinctly. Land-use activities had an impact on the local carbon dynamics, triggering soil
722 erosion and the outwash of SOC (Figure 4). With ongoing deforestation during the following Roman Period,
723 the effect of human pressure on the environment grew further.

Following the rise of the Roman city *Aventicum* south of the lake, large-scale agriculture with field cultivation made its entrance (Figure 2). Continuous soil degradation altered the sedimentary leaf wax distribution and $\delta^{13}C$ values, indicating enhanced input of terrestrial OM (Figure 4). Moreover, leaf wax radiocarbon dating revealed an increase in the mean transit time ($MTT_{lw}$) of the soil-derived compounds, suggesting that soil erosion was able to deplete the recalcitrant SOC pool. This supports the main findings from our previous study where we documented that outwash of soil OM due to soil erosion during the Early Roman Period was responsible for eutrophication of the lake, resulting in deposition of varved sediments.

After the fall of the Roman Empire human pressures decreased and a period of renaturation occurred. During the Great Migration Period ($4^{th}$ to $6^{th}$ century CE), land abandonment and a partial regrowth of the natural vegetation in the catchment helped stabilize the soils and remediated the SOC export back to pre-Roman values in approximately 200 years, as suggested by decreasing transit times of leaf waxes (Figure 4). A similar recovery rate was described in previous studies (Haas et al., 2019; Hillbrand et al., 2014). We assume that land-use was able to deplete the SOC pool, which might have resulted in long-lasting changes of the soil properties. For instance, we detected a significant shift in the plant community after the episode of Roman land-use, with mainly open, intensive to extensive cultivated area compared to the spacious woodlands (beech forests with silver fir and mixed oak elements) that existed during Neolithic times (Figure 3).

With the onset of Medieval agriculture (ca. 1000 CE) and the foundation of the city of Murten, a new wave of soil erosion and SOC outwash started. The following intensification of agriculture is visible not only in the pollen but also in the leaf wax record (Figure 3, 4). In particular, during the Industrial Period and the mechanization of agriculture a final but most prominent period of soil degradation was detected. During the modern land-use period, we assume soil erosion was also jointly responsible for recent eutrophication in Lake Murten that started around 1950.

***6. Acknowledgements:***

We would like to thank Serge Robert from Eawag, Silvia Bollhalder, Negar Haghipour and Lukas Wacker from the Laboratory of Ion Beam Physics at ETH Zürich and Marcel Bliedtner from the University of Jena for technical support during sample preparation, measurement and data interpretation. We would also like to thank Willy Tinner from the Institute of Plant Sciences at the University of Bern for facilitating the pollen analysis. Finally, we thank the Swiss National Science Foundation (SNSF) for funding the project "PALEOFARM": Grant Nr. 200021_160066/1.

## *7. Data Availability:*

Appendices A to F containing raw data tables are made available in the Mendeley data repository.

## *8. References:*

Ammann, B., 1989. Late-Glacial palynology at Lobsigensee. Regional vegetation history and local Lake development. Diss. Bot. 137, 1–157.

Behre, K.-E., 1988. The role of man in European vegetation history, in: Huntley, B., Webb, T. (Eds.), Vegetation History. Springer Netherlands, Dordrecht, pp. 633–672. https://doi.org/10.1007/978-94-009-3081-0_17

Bennett, K.D., 1996. Determination of the number of zones in a biostratigraphical sequence. New Phytol. 132, 155–170. https://doi.org/10.1111/j.1469-8137.1996.tb04521.x

Beug, H.J., 2004. Leitfaden der Pollenbestimmung für Mitteleuropa und angrenzende Gebiete. Publ. Verlag Friedrich Pfeil. https://doi.org/https://doi.org/10.1002/ardp.19622950723

Bichet, V., Gauthier, E., Massa, C., Perren, B., Richard, H., Petit, C., Mathieu, O., 2013. The history and impacts of farming activities in south Greenland: an insight from lake deposits. Polar Rec. (Gr. Brit). 49, 210–220. https://doi.org/https://doi.org/10.1017/S0032247412000587

Birks, H.J.B., Tinner, W., 2016. European tree dynamics and invasions during the Quaternary, in: Krumm, F., Vitkova, L. (Eds.), Introduced Tree Species in European Forests: Opportunities and Challenges. European Forest Institute, Freiburg, pp. 22–43. https://doi.org/citeulike-article-id:14216874

Blaauw, M., 2010. Methods and code for 'classical'age-modelling of radiocarbon sequences. Quat. Geochronol. 5, 512–518.

Blaauw, M., Christen, J.A., 2011. Flexible paleoclimate age-depth models using an autoregressive gamma process. Bayesian Anal. 6, 457–474. https://doi.org/10.1214/11-BA618

Bray, E.E., Evans, E.D., 1961. Distribution of n-paraffins as a clue to recognition of source beds. Geochim. Cosmochim. Acta 22, 2–15. https://doi.org/10.1016/0016-7037(61)90069-2

Bush, R.T., McInerney, F.A., 2013. Leaf wax n-alkane distributions in and across modern plants: Implications for paleoecology and chemotaxonomy. Geochim. Cosmochim. Acta 117, 161–179. https://doi.org/10.1016/J.GCA.2013.04.016

Butman, D.E., Wilson, H.F., Barnes, R.T., Xenopoulos, M.A., Raymond, P.A., 2015. Increased mobilization

787 of aged carbon to rivers by human disturbance. Nat. Geosci. 8, 112–116.
788 https://doi.org/10.1038/ngeo2322

789 Castella, D., Blank, P., Flück, M., Hufschmid, T., Krause, M.-F.M., 2015. Aventicum. Eine Römische
790 Hauptstadt. Association Pro Aventico.

791 Collister, J.W., Rieley, G., Stern, B., Eglinton, G., Fry, B., 1994. Compound-specific δ 13C analyses of leaf
792 lipids from plants with differing carbon dioxide metabolisms. Org. Geochem. 21, 619–627.
793 https://doi.org/10.1016/0146-6380(94)90008-6

794 Cugny, C., Mazier, F., Galop, D., 2010. Modern and fossil non-pollen palynomorphs from the Basque
795 mountains (western Pyrenees, France): the use of coprophilous fungi to reconstruct pastoral activity.
796 Veg. Hist. Archaeobot. 19, 391–408. https://doi.org/10.1007/s00334-010-0242-6

797 Diefendorf, A.F., Freimuth, E.J., 2017. Extracting the most from terrestrial plant-derived n-alkyl lipids and
798 their carbon isotopes from the sedimentary record: A review. Org. Geochem. 103, 1–21.
799 https://doi.org/10.1016/J.ORGGEOCHEM.2016.10.016

800 Diefendorf, A.F., Mueller, K.E., Wing, S.L., Koch, P.L., Freeman, K.H., 2010. Global patterns in leaf 13C
801 discrimination and implications for studies of past and future climate. Proc. Natl. Acad. Sci. U. S. A.
802 107, 5738–43. https://doi.org/10.1073/pnas.0910513107

803 Dietre, B., Walser, C., Kofler, W., Kothieringer, K., Hajdas, I., Lambers, K., Reitmaier, T., Haas, J.N., 2017.
804 Neolithic to Bronze Age (4850–3450 cal. BP) fire management of the Alpine Lower Engadine landscape
805 (Switzerland) to establish pastures and cereal fields. The Holocene 27, 181–196.
806 https://doi.org/10.1177/0959683616658523

807 Douglas, P.M.J., Pagani, M., Eglinton, T.I., Brenner, M., Curtis, J.H., Breckenridge, A., Johnston, K., 2018. A
808 long-term decrease in the persistence of soil carbon caused by ancient Maya land use. Nat. Geosci. 11,
809 645–649. https://doi.org/10.1038/s41561-018-0192-7

810 Douglas, P.M.J., Pagani, M., Eglinton, T.I., Brenner, M., Hodell, D.A., Curtis, J.H., Ma, K.F., Breckenridge,
811 A., 2014. Pre-aged plant waxes in tropical lake sediments and their influence on the chronology of
812 molecular paleoclimate proxy records. Geochim. Cosmochim. Acta 141, 346–364.
813 https://doi.org/10.1016/j.gca.2014.06.030

814 Dubois, N., Jacob, J., 2016. Molecular biomarkers of Anthropic impacts in natural archives: A review. Front.
815 Ecol. Evol. 4. https://doi.org/https://doi.org/10.3389/fevo.2016.00092

816 Edwards, K.J., Whittington, G., 2001. Lake sediments, erosion and landscape change during the Holocene in
817 Britain and Ireland. Catena 42, 143–173. https://doi.org/10.1016/S0341-8162(00)00136-3

818 Egli, H.-R., 1988. Some Thoughts on the Origin of the Open Field System in Switzerland and Its
819 Development in the Middle Ages. Geogr. Ann. Ser. B, Hum. Geogr. 70, 95–104.
820 https://doi.org/10.1080/04353684.1988.11879554

821 Eglinton, G., Hamilton, R.J., 1967. Leaf epicuticular waxes. Science (80-. ). 156, 1322–1335.
822 https://doi.org/10.1126/science.156.3780.1322

823 Eglinton, T.I., Eglinton, G., 2008. Molecular proxies for paleoclimatology. Earth Planet. Sci. Lett. 275, 1–16.

824 Enters, D., Lücke, A., Zolitschka, B., 2006. Effects of land-use change on deposition and composition of
825 organic matter in Frickenhauser See, northern Bavaria, Germany. Sci. Total Environ. 369, 178–187.

826 Farquhar, G., O'Leary, M., Berry, J., 1982. On the Relationship Between Carbon Isotope Discrimination and
827 the Intercellular Carbon Dioxide Concentration in Leaves. Aust. J. Plant Physiol. 13, 281–292.
828 https://doi.org/10.1071/PP9820121

Feng, X., Vonk, J.E., van Dongen, B.E., Gustafsson, O., Semiletov, I.P., Dudarev, O. V., Wang, Z., Montlucon, D.B., Wacker, L., Eglinton, T.I., 2013. Differential mobilization of terrestrial carbon pools in Eurasian Arctic river basins. Proc. Natl. Acad. Sci. 110, 14168–14173. https://doi.org/10.1073/pnas.1307031110

Ficken, K.., Li, B., Swain, D.., Eglinton, G., 2000. An n-alkane proxy for the sedimentary input of submerged/floating freshwater aquatic macrophytes. Org. Geochem. 31, 745–749. https://doi.org/10.1016/S0146-6380(00)00081-4

Finsinger, W., Tinner, W., 2005. Minimum count sums for charcoal-concentration estimates in pollen slides: Accuracy and potential errors. Holocene 15, 293–297. https://doi.org/10.1191/0959683605hl808rr

Foster, D., Swanson, F., Aber, J., Burke, I., Brokaw, N., Tilman, D., Knapp, A., 2003. The Importance of Land-Use Legacies to Ecology and Conservation. Bioscience 53, 77–88. https://doi.org/10.1641/0006-3568(2003)053[0077:tiolul]2.0.co;2

Fowler, A.J., Gillespie, R., Hedges, R.E.M., 1986. Radiocarbon Dating of Sediments. Radiocarbon 28, 441–450. https://doi.org/10.1017/S0033822200007578

Fry, B., Sherr, E.B., 1984. δ13C measurements as indicators of carbon flow in marine and fresh-water ecosystems. Contrib. Mar. Sci. 27, 13–47.

Galy, V., Eglinton, T., France-Lanord, C., Sylva, S., 2011. The provenance of vegetation and environmental signatures encoded in vascular plant biomarkers carried by the Ganges–Brahmaputra rivers. Earth Planet. Sci. Lett. 304, 1–12. https://doi.org/10.1016/J.EPSL.2011.02.003

Gierga, M., Hajdas, I., van Raden, U.J., Gilli, A., Wacker, L., Sturm, M., Bernasconi, S.M., Smittenberg, R.H., 2016. Long-stored soil carbon released by prehistoric land use: Evidence from compound-specific radiocarbon analysis on Soppensee lake sediments. Quat. Sci. Rev. 144, 123–131. https://doi.org/10.1016/J.QUASCIREV.2016.05.011

Haas, M., Baumann, F., Castella, D., Haghipour, N., Reusch, A., Strasser, M., Eglinton, T.I., Dubois, N., 2019. Roman-driven cultural eutrophication of Lake Murten, Switzerland. Earth Planet. Sci. Lett. 505, 110–117. https://doi.org/10.1016/J.EPSL.2018.10.027

Haas, M., Bliedtner, M., Borodynkin, I., Salazar, G., Szidat, S., Eglinton, T.I., Zech, R., 2017. Radiocarbon dating of leaf waxes in the Loess-Paleosol sequence Kurtak, central Siberia. Radiocarbon 59, 165–176. https://doi.org/10.1017/RDC.2017.1

Hadorn, P., 1992. Vegetationsgeschichtliche Studie am Nordufer des Lac de Neuchâtel: Pollenanalytische Untersuchungen im Loclat, in der Bucht von Hauterive/Saint-Blaise und in den neolithischen Ufersiedlungen von Saint-Blaise/Bain des Dames. Diss. Univ. Bern.

Hadorn, P., 1984. Pollenanalytische Untersuchungen über die jüngere nacheiszeitliche Vegetations- und Siedlungsgeschichte am Murtensee. Lizentiatsarbeit am Syst.-Geobot. Inst. der Univ. Bern.

Hanke, U.M., Wacker, L., Haghipour, N., Schmidt, M.W.I., Eglinton, T.I., McIntyre, C.P., 2017. Comprehensive radiocarbon analysis of benzene polycarboxylic acids (BPCAs) derived from pyrogenic carbon in environmental samples. Radiocarbon 59, 1103–1116. https://doi.org/10.1017/RDC.2017.44

Hillbrand, M., van Geel, B., Hasenfratz, A., Hadorn, P., Haas, J.N., 2014. Non-pollen palynomorphs show human- and livestock-induced eutrophication of Lake Nussbaumersee (Thurgau, Switzerland) since Neolithic times (3840 bc). Holocene 24, 559–568. https://doi.org/10.1177/0959683614522307

Huang, C.C., O'Connell, M., 2000. Recent land-use and soil-erosion history within a small catchment in Connemara, western Ireland: evidence from lake sediments and documentary sources. CATENA 41, 293–335. https://doi.org/10.1016/S0341-8162(00)00095-3

872 Juggins, S., 1991. ZONE software. Newcastle Universtiy Newcastle upon Tyne.

873 Lal, R., 2005. Soil erosion and carbon dynamics. Soil Tillage Res. 81, 137–142.
874 https://doi.org/10.1016/J.STILL.2004.09.002

875 Lal, R., 2004. Soil carbon sequestration impacts on global climate change and food security. Science (80-. ).
876 304, 1623–1627.

877 Lal, R., 2002. Soil carbon dynamics in cropland and rangeland. Environ. Pollut. 116, 353–362.
878 https://doi.org/10.1016/S0269-7491(01)00211-1

879 Magill, C.R., Ashley, G.M., Freeman, K.H., 2013. Ecosystem variability and early human habitats in eastern
880 Africa. Proc. Natl. Acad. Sci. U. S. A. 110, 1167–74. https://doi.org/10.1073/pnas.1206276110

881 Magny, M., 2004. Holocene climate variability as reflected by mid-European lake-level fluctuations and its
882 probable impact on prehistoric human settlements. Quat. Int. 113, 65–79. https://doi.org/10.1016/S1040-
883 6182(03)00080-6

884 Matsumoto, K., Kawamura, K., Uchida, M., Shibata, Y., 2007. Radiocarbon content and stable carbon
885 isotopic ratios of individual fatty acids in subsurface soil: Implication for selective microbial degradation
886 and modification of soil organic matter. Geochem. J. 41, 483–492.
887 https://doi.org/10.2343/geochemj.41.483

888 Mays, J.L., Brenner, M., Curtis, J.H., Curtis, K.V., Hodell, D.A., Correa-Metrio, A., Escobar, J., Dutton, A.L.,
889 Zimmerman, A.R., Guilderson, T.P., 2017. Stable carbon isotopes (δ13C) of total organic carbon and
890 long-chain n-alkanes as proxies for climate and environmental change in a sediment core from Lake
891 Petén-Itzá, Guatemala. J. Paleolimnol. 57, 307–319. https://doi.org/10.1007/s10933-017-9949-z

892 Menotti, F., 2004. Living on the lake in prehistoric Europe: 150 years of lake-dwelling research. Routledge.

893 Meyers, P.A., 1994. Preservation of elemental and isotopic source identification of sedimentary organic
894 matter. Chem. Geol. 114, 289–302. https://doi.org/10.1016/0009-2541(94)90059-0

895 Moore, P.D., Webb, J.A., Collison, M.E., 1991. Pollen analysis, 2nd ed. Blackwell Scientific Publications,
896 Oxford.

897 Nast, M., 2006. Überflutet - überlebt - überlistet: die Geschichte der Juragewässerkorrektionen. Verein
898 Schlossmuseum Nidau.

899 Pfiffner, O.A., 2014. Geology of the Alps. John Wiley & Sons.

900 Poynter, J.G., Eglinton, G., 1990. Molecular composition of three sediments from hole 717c: The Bengal fan.
901 Proc. Ocean Drill. Program, Sci. Results 116, 155–161.

902 Quinton, J.N., Govers, G., Van Oost, K., Bardgett, R.D., 2010. The impact of agricultural soil erosion on
903 biogeochemical cycling. Nat. Geosci. 3, 311–314. https://doi.org/10.1038/ngeo838

904 Reille, M., 1995. Pollen et spores d'Europe et d'Afrique du Nord: supplement 1. Marseille Lab. Bot. Hist.
905 Palynol. 274p.-illus.

906 Reimer, P.J., Bard, E., Bayliss, A., Beck, J.W., Blackwell, P.G., Ramsey, C.B., Buck, C.E., Cheng, H.,
907 Edwards, R.L., Friedrich, M., 2013. IntCal13 and Marine13 radiocarbon age calibration curves 0–50,000
908 years cal BP. Radiocarbon 55, 1869–1887.

909 Richoz, I., Haas, J.N., 1995. Flora und Vegetation im Neolithikum der Schweiz - Flore et végétation au
910 Néolithique en Suisse, in: Stöckli, W.E., Niffeler, U., Gross-Klee, E. (Eds.), Die Schweiz Vom
911 Paläolithikum Bis Zum Frühen Mittelalter: Bd. II: Neolithikum. Verlag Schweizerische Gesellschaft für
912 Ur- und Frühgeschichte, Basel, pp. 59–72.

913 Rieley, G., Collier, R.J., Jones, D.M., Eglinton, G., Eakin, P.A., Fallick, A.E., 1991. Sources of sedimentary
914 lipids deduced from stable carbon-isotope analyses of individual compounds. Nature 352, 425–427.
915 https://doi.org/10.1038/352425a0

916 Sachse, D., Radke, J., Gleixner, G., 2004. Hydrogen isotope ratios of recent lacustrine sedimentary n-alkanes
917 record modern climate variability. Geochim. Cosmochim. Acta 68, 4877–4889.
918 https://doi.org/10.1016/J.GCA.2004.06.004

919 Schibler, J., Jacomet, S., 2010. Short climatic fluctuations and their impact on human economies and
920 societies: the potential of the Neolithic lake shore settlements in the Alpine foreland. Environ. Archaeol.
921 15, 173–182.

922 Schöpfer, H., 2016. Murten (Gemeinde) [WWW Document]. Hist. Lex. der Schweiz. URL http://www.hls-
923 dhs-dss.ch/textes/d/D1014.php (accessed 9.18.18).

924 Schwörer, C., Kaltenrieder, P., Glur, L., Berlinger, M., Elbert, J., Frei, S., Gilli, A., Hafner, A., Anselmetti,
925 F.S., Grosjean, M., Tinner, W., 2014. Holocene climate, fire and vegetation dynamics at the treeline in
926 the Northwestern Swiss Alps. Veg. Hist. Archaeobot. 23, 479–496. https://doi.org/10.1007/s00334-013-
927 0411-5

928 Smittenberg, R.H., Eglinton, T.I., Schouten, S., Sinninghe Damsté, J.S., 2006. Ongoing buildup of refractory
929 organic carbon in boreal soils during the Holocene. Science (80-. ). 314, 1283–1286.
930 https://doi.org/10.1126/science.1129376

931 Soepboer, W., Sugita, S., Lotter, A.F., van Leeuwen, J.F.N., van der Knaap, W.O., 2007. Pollen productivity
932 estimates for quantitative reconstruction of vegetation cover on the Swiss Plateau. The Holocene 17, 65–
933 77. https://doi.org/10.1177/0959683607073279

934 Stockmarr, J.A., 1971. Tabletes with spores used in absolute pollen analysis. Pollen et Spores 615–621, 615–
935 621.

936 Tao, S., Eglinton, T.I., Montluçon, D.B., McIntyre, C., Zhao, M., 2015. Pre-aged soil organic carbon as a
937 major component of the Yellow River suspended load: Regional significance and global relevance. Earth
938 Planet. Sci. Lett. 414, 77–86. https://doi.org/10.1016/J.EPSL.2015.01.004

939 Tinner, W., Conedera, M., Ammann, B., Lotter, A.F., 2005. Fire ecology north and south of the Alps since the
940 last ice age. The Holocene 15, 1214–1226. https://doi.org/10.1191/0959683605hl892rp

941 Tinner, W., Hu, F.S., 2003. Size parameters, size-class distribution and area-number relationship of
942 microscopic charcoal: relevance for fire reconstruction. The Holocene 13, 499–505.
943 https://doi.org/10.1191/0959683603hl615rp

944 Tinner, W., Lotter, A.F., Ammann, B., Conedera, M., Hubschmid, P., van Leeuwen, J.F.N., Wehrli, M., 2003.
945 Climatic change and contemporaneous land-use phases north and south of the Alps 2300 BC to 800 AD.
946 Quat. Sci. Rev. 22, 1447–1460. https://doi.org/10.1016/S0277-3791(03)00083-0

947 Tinner, W., van der Knaap, W.O., Conedera, M., Ammann, B., 2018. Invasionen und Zusammenbrüche von
948 Baumarten nach der Eiszeit. Schweizerische Zeitschrift fur Forstwes.
949 https://doi.org/10.3188/szf.2018.0060

950 UNESCO Palafittes, 2015. UNESCO World Heritage - Prehistoric Pile Dwellings around the Alps [WWW
951 Document]. Int. Coord. Gr. UNESCO Palafittes. URL http://sites.palafittes.at/ (accessed 9.20.18).

952 van Bree, L.G.J., Peterse, F., van der Meer, M.T.J., Middelburg, J.J., Negash, A.M.D., De Crop, W., Cocquyt,
953 C., Wieringa, J.J., Verschuren, D., Sinninghe Damsté, J.S., 2018. Seasonal variability in the abundance
954 and stable carbon-isotopic composition of lipid biomarkers in suspended particulate matter from a
955 stratified equatorial lake (Lake Chala, Kenya/Tanzania): Implications for the sedimentary record. Quat.
956 Sci. Rev. 192, 208–224. https://doi.org/10.1016/J.QUASCIREV.2018.05.023

van Geel, B., Buurman, J., Brinkkemper, O., Schelvis, J., Aptroot, A., van Reenen, G., Hakbijl, T., 2003. Environmental reconstruction of a Roman period settlement site in Uitgeest (the Netherlands), with special reference to coprophilous fungi. J. Archaeol. Sci. 30, 873–883. https://doi.org/10.1016/S0305-4403(02)00265-0

Van Oost, K., Quine, T.A., Govers, G., De Gryze, S., Six, J., Harden, J.W., Ritchie, J.C., McCarty, G.W., Heckrath, G., Kosmas, C., Giraldez, J. V, da Silva, J.R.M., Merckx, R., 2007. The impact of agricultural soil erosion on the global carbon cycle. Science (80-. ). 318, 626–629. https://doi.org/10.1126/science.1145724

Volkman, J.K., Johns, R.B., Gillan, F.T., Perry, G.J., Bavor, H.J., 1980. Microbial lipids of an intertidal sediment—I. Fatty acids and hydrocarbons. Geochim. Cosmochim. Acta 44, 1133–1143. https://doi.org/10.1016/0016-7037(80)90067-8

Vonk, J.E., van Dongen, B.E., Gustafsson, Ö., 2010. Selective preservation of old organic carbon fluvially released from sub-Arctic soils. Geophys. Res. Lett. 37. https://doi.org/10.1029/2010GL042909

Wacker, L., Fahrni, S.M., Hajdas, I., Molnar, M., Synal, H.A., Szidat, S., Zhang, Y.L., 2013. A versatile gas interface for routine radiocarbon analysis with a gas ion source, in: Zondervan, A., Prior, C., Bruhn, F., Sparks, R. (Eds.), Nuclear Instruments and Methods in Physics Research Section B: Beam Interactions with Materials and Atoms. pp. 315–319. https://doi.org/10.1016/j.nimb.2012.02.009

Wehrli, M., Tinner, W., Ammann, B., 2007. 16 000 years of vegetation and settlement history from Egelsee (Menzingen, central Switzerland). The Holocene 17, 747–761. https://doi.org/10.1177/0959683607080515

Yamamoto, S., Kawamura, K., Seki, O., Meyers, P.A., Zheng, Y., Zhou, W., 2010. Environmental influences over the last 16 ka on compound-specific δ13C variations of leaf wax n-alkanes in the Hani peat deposit from northeast China. Chem. Geol. 277, 261–268. https://doi.org/10.1016/J.CHEMGEO.2010.08.009

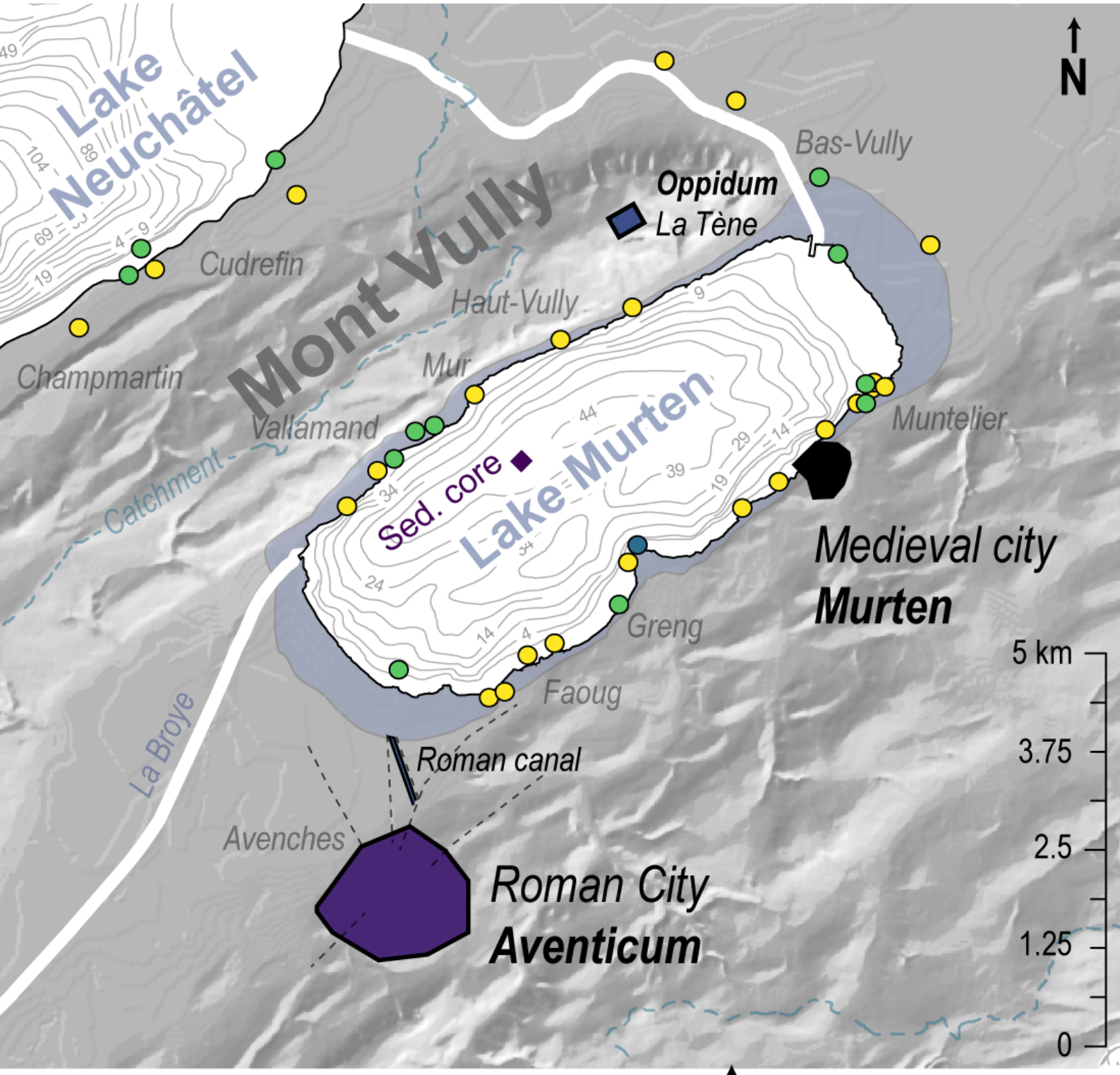


**Archaeological Overview**

- Pile dwelling site
- Roman roads
- Lake shore reconstruction (1 CE)

- ***Medieval Period***, 5th - 15th century CE
- ***Roman Period***, 20 BCE - 5th century CE
- ***Late Iron Age*** (La Tène), 450 - 20 BCE
- ***Early Iron Age*** (Hallstatt), 800 - 450 BCE
- ***Bronze Age***, 2200 - 800 BCE
- ***Neolithic Period***, 5500 - 2200 BCE

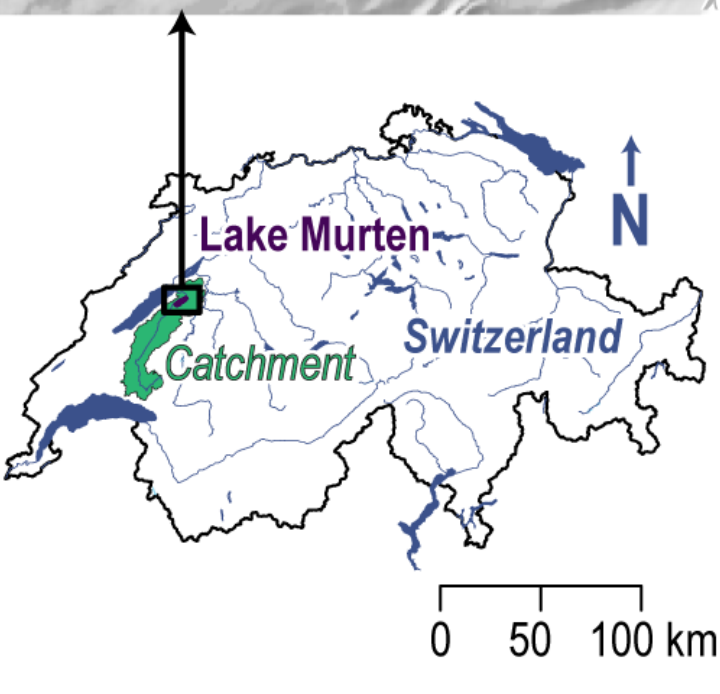

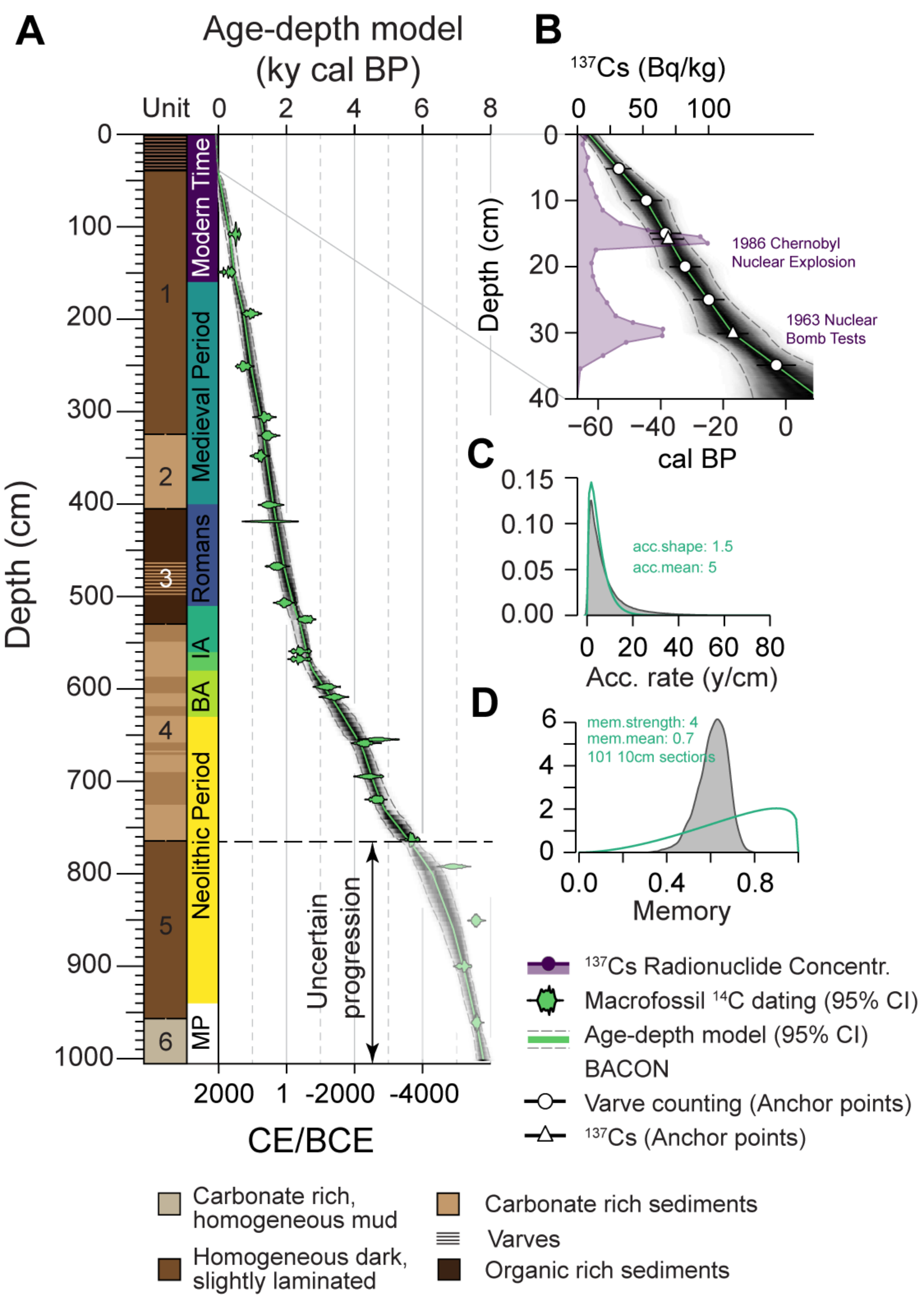
A
Age-depth model
(ky cal BP)
Unit
0
2
4
6
8
Depth (cm)
0
100
200
300
400
500
600
700
800
900
1000
Modern Time
Medieval Period
Romans
IA
BA
Neolithic Period
MP
1
2
3
4
5
6
Uncertain
progression
2000
1
-2000
-4000
CE/BCE
B
137Cs (Bq/kg)
0
50
100
Depth (cm)
0
10
20
30
40
1986 Chernobyl
Nuclear Explosion
1963 Nuclear
Bomb Tests
−60
−40
−20
0
cal BP
C
0.15
0.10
0.05
0.00
acc.shape: 1.5
acc.mean: 5
0
20
40
60
80
Acc. rate (y/cm)
D
6
4
2
0
mem.strength: 4
mem.mean: 0.7
101 10cm sections
0.0
0.4
0.8
Memory
137Cs Radionuclide Concentr.
Macrofossil 14C dating (95% CI)
Age-depth model (95% CI)
BACON
Varve counting (Anchor points)
137Cs (Anchor points)
Carbonate rich,
homogeneous mud
Homogeneous dark,
slightly laminated
Carbonate rich sediments
Varves
Organic rich sediments

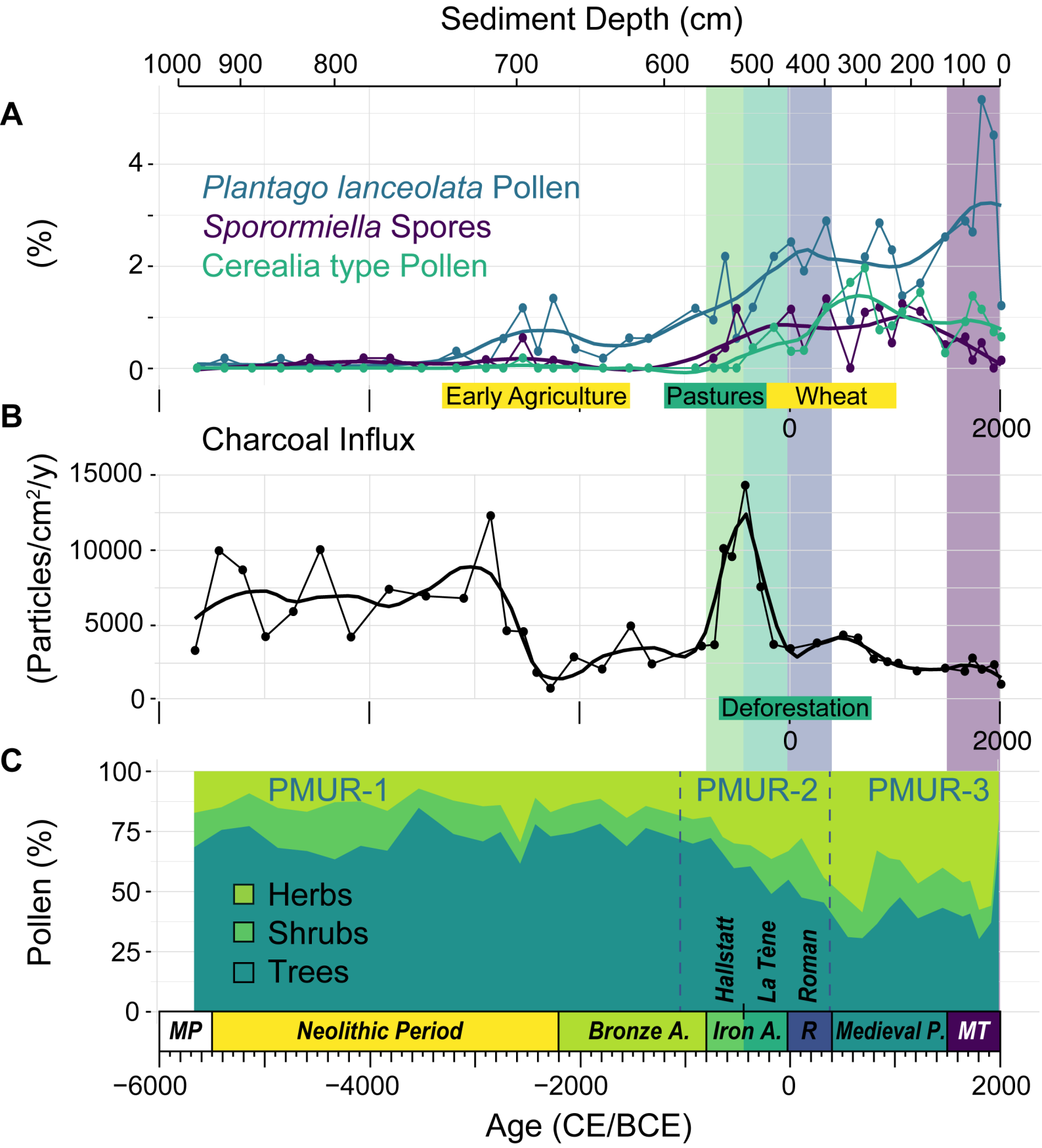
Sediment Depth (cm)
1000 900 800 700 600 500 400 300 200 100 0
A
(%)
4
2
0
Plantago lanceolata Pollen
Sporormiella Spores
Cerealia type Pollen
Early Agriculture
Pastures
Wheat
B
Charcoal Influx
(Particles/cm²/y)
15000
10000
5000
0
Deforestation
0
2000
C
Pollen (%)
100
75
50
25
0
PMUR-1
PMUR-2
PMUR-3
Herbs
Shrubs
Trees
Hallstatt
La Tène
Roman
MP
Neolithic Period
Bronze A.
Iron A.
R
Medieval P.
MT
−6000
−4000
−2000
0
2000
Age (CE/BCE)

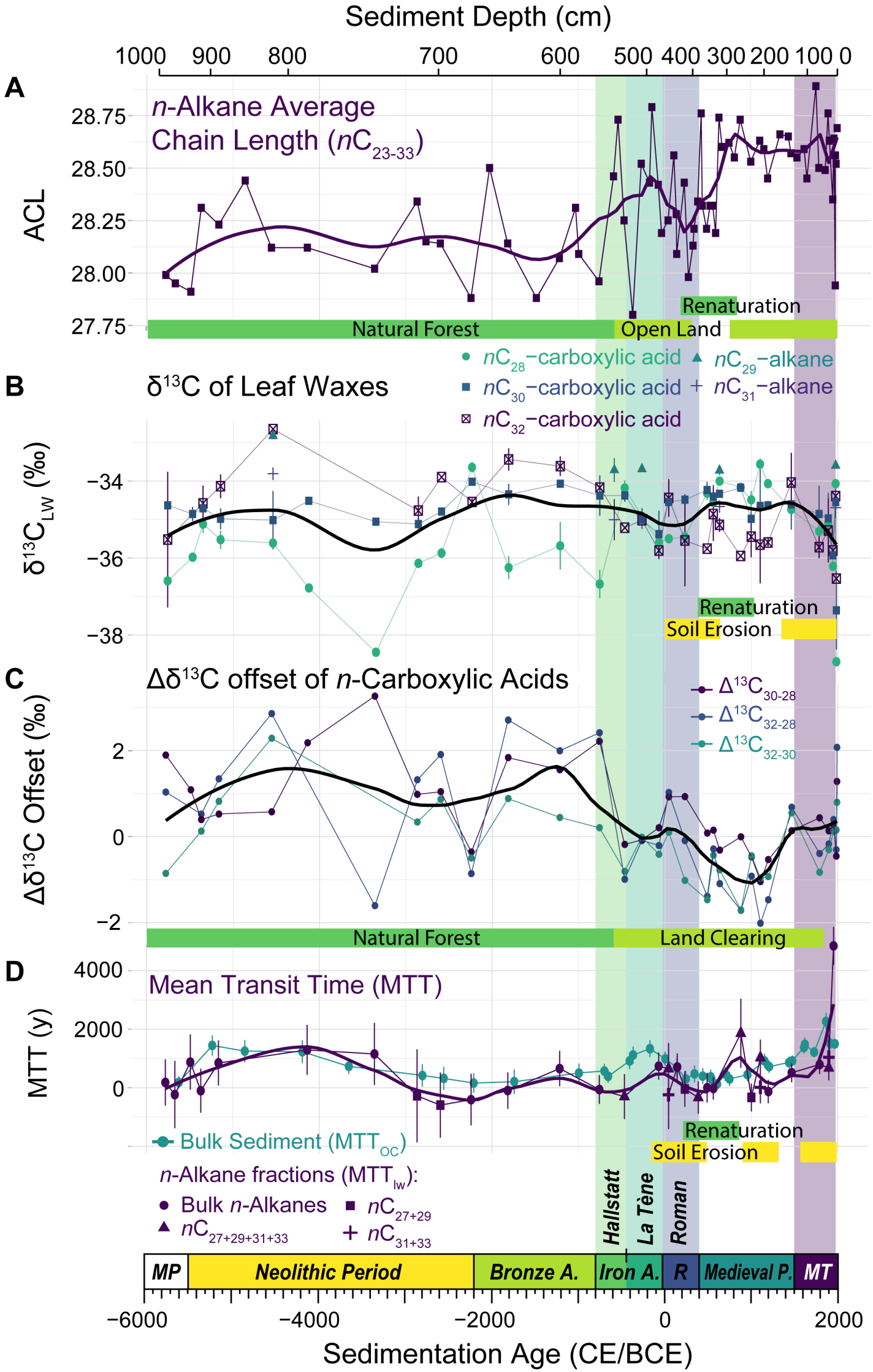
Sediment Depth (cm)
1000 900 800 700 600 500 400 300 200 100 0
A
n-Alkane Average Chain Length (nC23-33)
ACL
28.75
28.50
28.25
28.00
27.75
Renaturation
Natural Forest
Open Land
nC28−carboxylic acid
nC29−alkane
nC30−carboxylic acid
nC31−alkane
nC32−carboxylic acid
B
δ13C of Leaf Waxes
δ13CLW (‰)
−34
−36
−38
Renaturation
Soil Erosion
C
Δδ13C offset of n-Carboxylic Acids
Δδ13C Offset (‰)
Δ13C30-28
Δ13C32-28
Δ13C32-30
2
0
−2
Natural Forest
Land Clearing
D
Mean Transit Time (MTT)
MTT (y)
4000
2000
0
Renaturation
Soil Erosion
Bulk Sediment (MTTOC)
n-Alkane fractions (MTTlw):
Bulk n-Alkanes
nC27+29
nC27+29+31+33
nC31+33
Hallstatt
La Tène
Roman
MP
Neolithic Period
Bronze A.
Iron A.
R
Medieval P.
MT
−6000 −4000 −2000 0 2000
Sedimentation Age (CE/BCE)